YAĞMUR BUDAK

ATILIM UNIVERSITY

# DESIGN, MANUFACTURING AND TESTING OF HIGH TEMPERATURE PEM FUEL CELL STACK

YAĞMUR BUDAK

JANUARY 2019

# DESIGN, MANUFACTURING AND TESTING OF HIGH TEMPERATURE PEM FUEL CELL STACK

A THESIS SUBMITTED TO
THE GRADUATE SCHOOL OF NATURAL AND APPLIED SCIENCES
OF
ATILIM UNIVERSITY

BY

YAĞMUR BUDAK

IN PARTIAL FULFILLMENT OF THE REQUIREMENTS
FOR
THE DEGREE OF MASTER OF SCIENCE
IN
THE DEPARTMENT OF MANUFACTURING ENGINEERING

JANUARY 2019

Approval of the Graduate School of Natural and Applied Sciences, Atilim University.

_____

Prof. Dr. Ali KARA
Director

I certify that this thesis satisfies all the requirements as a thesis for the degree of **Master of Science in Manufacturing Engineering, Atilim University**.

_____

Prof. Dr. Engin S. KILIÇ
Head of Department

This is to certify that we have read the thesis DESIGN, MANUFACTURING AND TESTING OF HIGH TEMPERATURE PEM FUEL CELL STACK submitted by Yağmur BUDAK and that in our opinion it is fully adequate, in scope and quality, as a thesis for the degree of Master of Science.

_____

Assoc. Prof. Dr. Yılser DEVRİM
Supervisor

**Examining Committee Members:**

Assoc. Prof. Dr. Yılser DEVRİM
Energy Systems Engineering Dept. Atilim University _____

Assoc. Prof. Dr. Hakan Ahmet ARGEŞO
Manufacturing Dept. Atilim University _____

Asst.Dr. Muhittin BİLGİLİ
Mechanical Engineering Dept. Gazi University _____

**Date:** 30.01.2019

I hereby declare that all information in this document has been obtained and presented in accordance with academic rules and ethical conduct. I also declare that, as required by these rules and conduct, I have fully cited and referenced all materials and results that are not original to this work.

Name, Last Name: Yağmur Budak

Signature:

## ABSTRACT

### DESIGNING, MANUFACTURING AND TESTING OF HIGH TEMPERATURE PEM FUEL CELL

Budak, Yağmur

M.S., Manufacturing Engineering Department

Supervisor: Assoc. Prof. Dr. Yılser Devrim

January 2019, 66 pages

In recent years, the need for energy has been increasing with the developing of technology and population. The proton exchange membrane fuel cell (PEMFC) considered to be the preferred alternative energy technology in recent years due to its high efficiency, low emission, high power density, quiet operation and short start-up period. High Temperature PEMFC (HT-PEMFC) type PEMFC provide easy water management and high carbon monoxide (CO) tolerance thanks to over 100 ºC of operation temperature. PEMFC must have high CO tolerances for PEMFC commercialization and usage of reformed gases obtained from a short process of gases such as natural gas and methane, which are frequently used today.

In this thesis, the design, manufacturing and testing of a nominal 300 W HT-PEMFC stack which has 150 $cm^2$ active area and 12 cells were performed. The materials chosen to manufacture this stack are composite graphite bipolar plates, eloxal coated aluminum plates, Gold-coated copper plate current collectors, stainless steel connections, Viton® gasket, Pt/C coated carbon paper gas diffusion layer and PBI membranes.

In the scope of the thesis, the current test station was upgraded in order to test HT-PEMFC stack by reformate gas mixture. Firstly, a single HT-PEMFC performance test was performed with Hydrogen ($H_2$) gas and reformate gas mixture supply at 160$^oC$ in order to obtain the design parameters of the stack would be produced. The current density value at 0.6 V was obtained as 0.33 A/cm$^2$ with $H_2$ supply, and 0.28 A/cm$^2$ was obtained with reformate gas mixture supply. Then, according to single HT-PEMFC test result, the stack of HT-PEMFC was designed. After the design of the stack, the pressure drop on the bipolar plate was analyzed for 3 different gas flow rates using Solid Works® Flow Simulation program. The pressure losses were determined maximum 83.5 Pa for $H_2$ at 0.5 slpm and 129.83 Pa to reformate gas mixture ($H_2$/$CO_2$/CO;75/22/3) at 0.56 slpm. After that, the performance of stack produced were tested by pure $H_2$ and reformate gas mixture supply. The stack power with pure $H_2$ feed was 320 W at 7.2 V operation voltage, it was 218 W at 7.2 V for reformate gas mixture. In addition, with the $H_2$ supply, the total efficiency of the stack was 79 %, while this efficiency decreases to 76 % with its reformate gas mixture supply. These losses can be ignored considering the advantages of reformate gas mixture use and the importance of fuel cell for commercialization.

Keywords: High Temperature Fuel Cell, PBI, Flow Analysis, Stack Production, Performance Tests

# ÖZ

## YÜKSEK SICAKLIK PEM YAKIT HÜCRESİ YIĞINI TASARIMI, ÜRETİMİ VE TESTLERİ

Budak, Yağmur
Yüksek Lisans, İmalat Mühendisliği Bölümü
Tez Yöneticisi: Doç. Dr. Yılser Devrim

Ocak 2019, 66 Sayfa

Son yıllarda, teknoloji ve nüfusun gelişmesiyle birlikte enerjiye olan ihtiyaç da artmaktadır. Proton Değişim Membran Yakıt Hücreleri (PEMFC), yüksek verimlilikleri, düşük emisyon üretmeleri, yüksek güç yoğunlukları, sessiz çalışmaları ve kısa başlangıç süreleri sayesinde son yıllarda oldukça tercih edilen alternatif enerji teknolojilerinden birisidir. Yüksek Sıcaklık PEMFC (HT-PEMFC) tipi PEMFC, 100 derecenin üzerindeki çalışma sıcaklıkları sayesinde kolay su yönetimi ve yüksek karbon monoksit (CO) toleransı sağlarlar. Bu tip yakıt hücrelerinin günümüzde sıklıkla kullanılan doğal gaz ve metan gibi gazların kısa bir işleminden elde edilen reformat gazlar ile kullanılabilmeleri ve daha kolay ticarileşmeleri için CO toleranslarının büyük olması gerekmektedir.

Bu tez çalışmasında, 150 $cm^2$ aktif alana ve 12 hücreye sahip nominal bir 300 W HT-PEMFC yığınının tasarımı, üretimi ve testleri yapılmıştır. HT-PEMFC yığınının üretimi için seçilen malzemeler; kompozit grafit bipolar plakalar, eloksal kaplı alüminyum plakalar, Altın kaplı bakır plaka akım toplayıcıları, paslanmaz çelik bağlantılar, Viton® conta, Pt/C kaplı karbon kâğıt gaz difüzyon tabakası ve PBI membranlarıdır.

Tez kapsamında, mevcut test istasyonu HT-PEMFC yığınını reformat gaz karışımı ile test edebilmek amacıyla geliştirilmiştir. Yığının tasarım parametrelerinin belirlenebilmesi için ilk olarak 160$^{o}$C'de Hidrojen ($H_2$) gazı ve reformat gaz karışımı beslemesi ile tek hücreli performans testleri yapılmıştır. 0.6 V çalışma voltajında $H_2$ gazı ile 0.33 A/cm$^2$ ve reformat gaz karışımı ile 0.28 A/cm$^2$ akım yoğunluğu değerleri elde edilmiştir. Daha sonra tek hücreli HT-PEMFC'in test sonucuna göre HT-PEMFC yığını tasarımı yapılmıştır. Yığın tasarımının ardından bipolar plaka üzerindeki basınç kaybı, Solidwork Flow Simulation programı kullanılarak 3 farklı gaz akış hızı için analiz edilmiştir. Maximum basınç kayıpları, $H_2$ ve reformat gaz karışımı ($H_2$/$CO_2$/CO-75/22/3) için sırasıyla 0.5 slpm de 83.5 Pa ve 0.56 slpm de 129.83 Pa olarak hesaplanmıştır. Ardından üretilen yığın performansları $H_2$ ve reformat gaz ile test edilmiştir. Saf $H_2$ beslemeli HT-PEMFC yığınının gücü 7.2 V çalışma voltajında 320 W iken, reform gaz karışımı ile HT-PEMFC yığınının gücü 7.2 V'da 218 W elde edilmiştir. Buna ek olarak, $H_2$ beslemesi ile yığının toplam verimi %79 olarak belirlenirken, reformat gaz beslemesi ile verim % 76'ya düşmektedir. Bu kayıplar, reformat gaz karışımı kullanımının avantajları ve yakıt hücresinin ticarileşmesi göz önüne alındığında ihmal edilebilecek kayıplarıdır.

Anahtar Kelimeler: Yüksek Sıcaklık Yakıt Hücresi, PBI, Akış analizi, Yığın Üretimi, Performans Testleri

To My Family

## ACKNOWLEDGMENTS

I would like to express my deepest gratitude to supervisor Assoc. Prof. Dr. Yılser Devrim for her guidance, advice, criticism, encouragements and insight throughout the research. My biggest thank to her is teaching me the fuel cells, strengthening my love for my profession and opening my way.

Special thanks to the Hüseyin Devrim and Ömer Erdemir from TEKSİS Ltd. Şti. for their support.

I shall also thank to my friends Gökhan Çakır and Kübra Pehlivanoğlu for answering my questions about the Solidworks® Flow Simulation program. Also I would like to thank to the lab collegue Yağmur Özdemir for her support and preparing PBI polymers.

I would like to thank my dear friends Feride Cansu İskenderoğlu, Şebnem Akar, Öykü Odabaş, and all my friends who cannot write their names for their friendships, support and smile.

I am grateful to my family for their patience and efforts and moral supports.

This study is supported by the Scientific and Technological Research Council of Turkey (TUBITAK) 1001 Project (Grant number: 214M301).

## TABLE OF CONTENTS

## LIST OF TABLES

## LIST OF FIGURES

## LIST OF SYMBOLS/ABBREVIATIONS

| | |
|---|---|
| $CaCl_2$ | Calcium Chloride |
| $C_B$ | Bulk Concentration of Reactant |
| CCM | Carbon Coated Membrane |
| $CH_3C(O)N(CH_3)_2$ DMAc | N-N dimethylacetamide |
| CL | Catalyst Layer |
| CO | Carbon Monoxide |
| $CO_2$ | Carbon Dioxide |
| $CO_3^{-2}$ | Carbonate |
| DI | Deionized Water |
| D | Diffusion Coefficient of The Reacting Species |
| DAB | 3,3'-Diaminobenzidine |
| DAB.4HCl.$2H_2O$ | Diaminobenzidine Tetrachloride Hydrate |
| E | Potential |
| $E_r$ | Equilibrium or Reversible Potential |
| F | Faraday Constant (A.s/mole) |
| G | Gibbs Energy of Activation |
| $G_b$ | Gibbs Oxidation Reaction |
| $G_{ch}$ | Gibbs Chemical Component |
| $G_f$ | Gibbs Reduction Energy |
| h | Plank's Constant |
| $H_2$ | Hydrogen |
| $H_2O$ | Water |
| $H_2SO_4$ | Sulfuric Acid |
| $H_3PO_4$ | Phosphoric Acid |
| I | Current |
| ICR | Interface Contact Resistance |
| IPA | Isophthalic Acid |
| k | Heterogeneous Rate Coefficient |

| | |
|---|---|
| $K_2CO_3$ | Potassium Carbonate |
| $k_B$ | Boltzmann's Constant (J/K) |
| $KMnO_4$ | Potassium Permanganate |
| KOH | Potassium Hydroxide |
| $Li_2CO_3$ | Lithium Carbonate |
| n | Number of Electrons per Molecule |
| $O_2$ | Oxygen |
| $OH^-$ | Hydroxide |
| OCV | Open Circuit Voltage |
| PBI | Poly(2,2-(m-phenylene)-5,5-bibenzimidazole |
| PTFE | Polytetrafluoroethylene |
| PVDF | Polyvinylidene Difluoride |
| $R_i$ | İnternal Resistance |
| R | İdeal Gas Constant |
| SiC | Silicon Carbide |
| T | Temperature (°C) |
| TPA | Terephthalic Acid |
| $\Delta V_{act}$ | Activation Polarization (V) |
| $\Delta V_{conc:}$ | Concentration Polarization (V) |
| $\Delta V_{ohm:}$ | Ohmic Losses (V) |
| $W_{H3PO4}$ | Weight of Acid Doped Membrane(g) |
| $W_{dry}$ | weight of Dry Membrane (g) |
| $W_0$ | Initial Weight of Acid Doped Membrane (g) |
| Wi | Membrane Weight After Leaching (g) |
| Wa | Weight of $H_3PO_4$ Present in The Membrane (g) |
| AFC | Alkaline Fuel Cell |
| BoP | Balance of Plant |
| PEMFC | Proton Exchange Membrane Fuel Cell |
| LT-PEMFC | Low Temperature PEMFC |
| HT-PEMFC | High Temperature PEMFC |
| MCFC | Molten Carbonate Cell Fuel |
| SOFC | Solid Oxide Fuel Cell |

| | |
|---|---|
| PAFC | Phosphoric Acid Fuel Cell |
| MEA | Membrane Electrode Assembly |
| GDE | Gas Diffusion Electrode |
| GDL | Gas Diffusion Layer |
| PPA | Polyphosphoric Acid |
| CHP | Combine Heat and Power |
| MFC | Mass Flow Controller |
| $C_p$ | Specific Heats (kJ/kg $^oC$) |
| N | Molar Flow Rates of Gases (mole/s) |
| $\Delta h$ | Low Heating Value of Hydrogen |
| $P_{H2}$ | Chemical Power of Hydrogen (W) |
| $P_{coolant}$ | Coolant Power (W) |
| $P_{out}$ | Stack Output Power (W) |
| $\dot{E}_{mass,in}$ | Enthalpy of Inlet Gases (W) |
| $\dot{E}_{mass,out}$ | Enthalpy of Outlet Gases (W) |
| Q | Heat Dissipation from The PEMFC Stacks (W) |
| $W_{net}$ | Net Power Production by PEMFC Stacks (W) |
| $\alpha$ | Transfer Coefficient |
| $\beta$ | Transfer Coefficient |
| $\delta$ | Diffusion Distance |
| $\eta$ | Efficiency |

# CHAPTER 1

# 1. INTRODUCTION

## 1.1. Fuel Cell

The need for energy increases with increasing world population and technological developments. Thus, the production and use of energy with low cost, sustainable and renewable fuels for global stability and peace is gaining importance. As a country's energy consumption increases, the economic and social development of that country gains momentum [1]. Due to these reasons, progress of renewable energy systems is necessary. Fuel cells are devices that produce electrical energy with using chemical energy without the need for combustion. Without the combustion, the high energy losses and harmful emissions which are usually combined with the combustion process are eliminated [2].

Fuel cells have an electrolyte layer between two electrodes. Anode side of the electrode is fed with the fuel and the cathode side of the electrode is fed with the oxidant, continuously. At the anode side the fuel is ionized to positive and negative ions. The membranes forming the electrolyte layer act as an insulator for electrons and prevent their passage while allowing only positive ions to pass through the anode to the cathode. These electrons are recombined on the other side of the membrane to be stable system by passing through an external electric circuit to the cathode side. Positive and negative ions combine with the oxidant to form a depleted oxidant (or/and) pure water on the cathode side [3].

The first fuel cell was investigated by Sir William Grove in 1839. He named the system as ‘gaseous voltaic battery’ then developed this investment in 1849 that produced electrical energy by combining Hydrogen ($H_2$) and Oxygen ($O_2$).

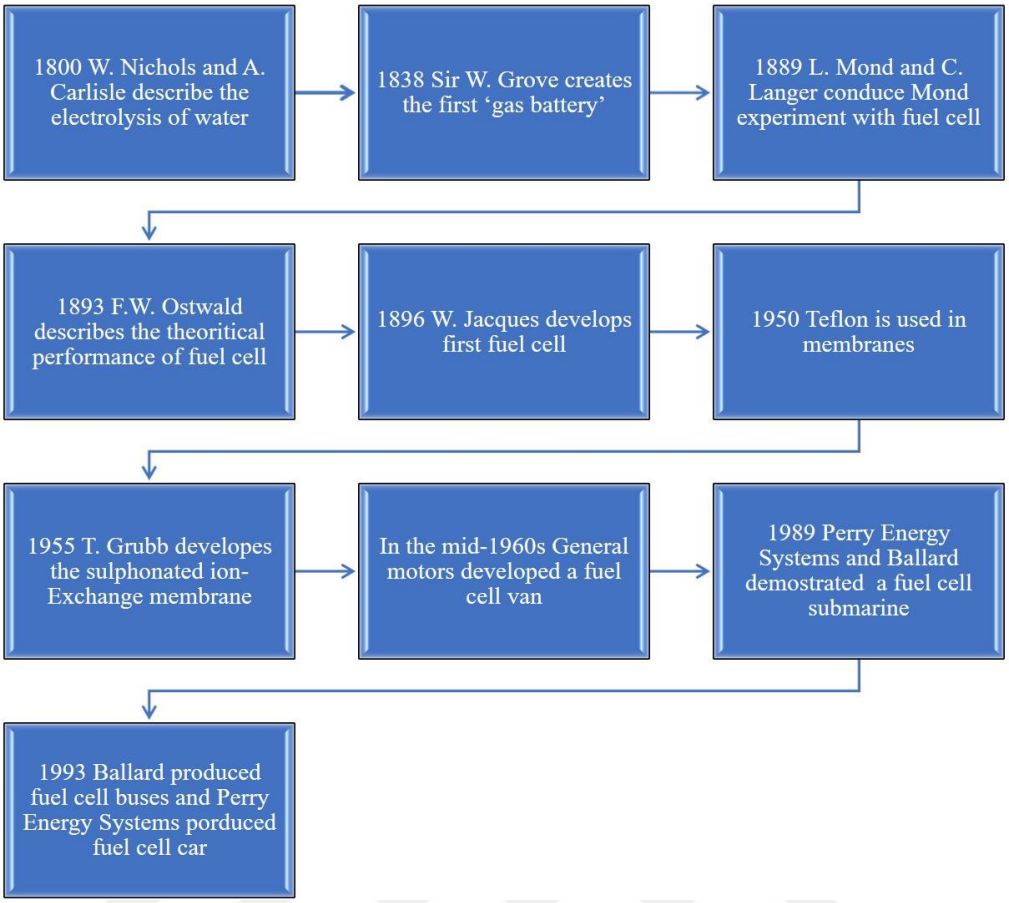


Figure 1.1.Historical development of fuel cell [4]

In the invention, the sulfuric acid water electrolyte was electrolyzed to the $H_2$ and $O_2$ by electricity and the produced gases were stored in the suitable electrodes of the series-connected cells. When disconnecting the electric power, the electrolysis was stopped. By the time a single electrolysis cell is connected the series cells, $H_2$ and $O_2$ were converted back to water at the platinum electrodes [4]. Even though WF Ostwald, who received the Nobel Prize in 1909 and was the founder of the physical chemistry field, provided theoretical knowledge about how fuel cells work, it has not been a scientific interest for a century. First fuel cell stack completed construction and evaluation by Francis T. Bacon in 1952 [5]. A short diagram about the historical development of fuel cell is shown in Figure 1.1.

## 1.2. Types of the Fuel Cell

Fuel cells are separated into five types by the kind of electrolyte as shown in Table 1.1.

### 1.2.1. Alkaline Fuel Cell (AFC)

AFC produces electrical energy in aqueous solution using alkaline electrolyte potassium hydroxide (KOH). The existence of hydroxyl ions moving along the electrolyte creates a circuit and electric energy can be obtained. The operating temperature of the AFCs is higher than 60°C. It has able to work at lower temperatures with recent technologies. Nickel-type catalysts are used to accelerate electrochemical reactions on the cathode and anode side. The electrical efficiency of the AFCs is about 50 % and when the produced heat is used, this efficiency rises above 80 % [6]. AFCs are preferred in military, aerospace, reserve power and transportation areas due to their wider range of stable materials, lower cost components, working in low temperature and fast start up. But they have some difficulties such as sensitive to $CO_2$ in fuel and air, aqueous electrolyte management.

### 1.2.2. Phosphoric Acid Fuel Cell (PAFC)

PAFC was the first commercially available fuel cell. PAFC consists of a porous matrix surrounded by porous carbon electrodes, which holds the liquid phosphoric acid electrolyte. Apart from the nature of the electrolyte, the PAFC structure is similar to the Proton Exchange Membrane Fuel Cell (PEMFC) with porous carbon electrodes and carbon gas diffusion layer which is located on either side of the Membrane Electrode Assembly (MEA). When PAFC is compared to PEMFC, the efficiencies are nearly same but power densities are lower. They have high tolerance to fuel impurities and their operating temperature is suffice to facilitate the micro-cogeneration (μCHP), but the operating temperature is not high suffice to overcome the requirement for precious metal catalysts [7]. Also, they have sulfur sensitivity and because of their working temperature, the startup time is long.

### 1.2.3. Molten Carbonate Fuel Cell (MCFC)

MCFC electrolyte is a molten mixture of alkali metal carbonates, lithium carbonate ($Li_2CO_3$) and potassium carbonate ($K_2CO_3$) retrained in a porous ceramic matrix of $LiAlO_2$. MCFCs can be fitted facilities for internal reforming process which directly converts hydrocarbon to $H_2$ within the fuel cell by quality of their high operating temperatures. Thus, MCFC systems can use gaseous hydrocarbons such as methane, methanol and petroleum or gasified coal. MCFC electrodes are nickel based which provide catalytic activity and conductivity. They can be used with μCHP and hybrid gas turbine cycle. The main disadvantage of MCFC originate from using a highly corrosive and molten electrolyte [8].

### 1.2.4. Solid Oxide Fuel cell (SOFC)

A SOFC system generally use a solid ceramic as the electrolyte and working at ultrahigh temperatures. This high working temperature enable internal reforming, allow rapid electrocatalysis with non-precious metals, and produce extremely high heat for μCHP. Total efficiency can increase to 70 % with μCHP for this type of fuel cell. SOFC can be come in handy in industrial stations and electricity generating stations which are generated high powers [9].

### 1.2.5. Proton Exchange Membrane Fuel Cell

A PEMFC use a polymer membrane as an electrolyte. Polymer membranes are excellent conductors of $H_2$ ions even if they are electronic insulators. Until today, the materials used consist of a fluorocarbon polymer basis, similar to Teflon that sulfonic acid groups are bounded. Acid molecules bind to the polymer to cannot to leak but these acid groups protons are free to transport through the membrane. The loss of electrolyte is no longer a problem with the use of solid-type polymer electrolyte [10].

Proton Exchange Membrane (PEM) type is one of the most preferred types because of their advantages. PEMFC has two types which are separated according to their working temperature. The working temperatures effect the usage areas. Low

Temperature PEMFC (LT-PEMFC) are working between the temperatures 60-80ºC, High Temperature PEMFC (HT-PEMFC) working the temperature higher than 100ºC [11].

Table 1.1.Types of Fuel Cell [12]

| Fuel Cell | Mobile Ion | Operating Temp. (°C) | Overall Reaction Process | Electrical Efficiency (%) | Power Level (kW) |
|---|---|---|---|---|---|
| **AFC** | $OH^-$ | 60-220 | $H_2+½O_2 \rightarrow H_2O$ | 50 | 10-100 |
| **PAFC** | $H^+$ | 200 | $H_2+½O_2 \rightarrow H_2O$ | 40 | 100-5000 |
| **MCFC** | $CO_3^{-2}$ | 650 | $H_2+½\ O_2+CO_2 \rightarrow H_2O + CO_2$ | 45-55 | 1000-100000 |
| **SOFC** | $O^-$ | 600-1000 | $H_2+½O_2 \rightarrow H_2O$ | 50-60 | 100-100000 |
| **PEMC** | $H^+$ | 60-80 | $H_2+½O_2 \rightarrow H_2O$ | 40-50 | 0.1 - 1000 |

# CHAPTER 2

## 2. PEMFC

### 2.1. Operation of PEMFC

PEMFC has electrochemical reaction both anode and cathode sides of the cell. The operation method of PEMFC is shown in Figure 2.1. The reactions are given in the below:

Anode reaction: $H_2 \rightarrow H^+ + 2e^-$ (1)

Cathode reaction: $\frac{1}{2}O_2 + H^+ + 2e^- \rightarrow H_2O$ (2)

Overall cell reaction: $H_2 + \frac{1}{2}O_2 \rightarrow H_2O$ (3)

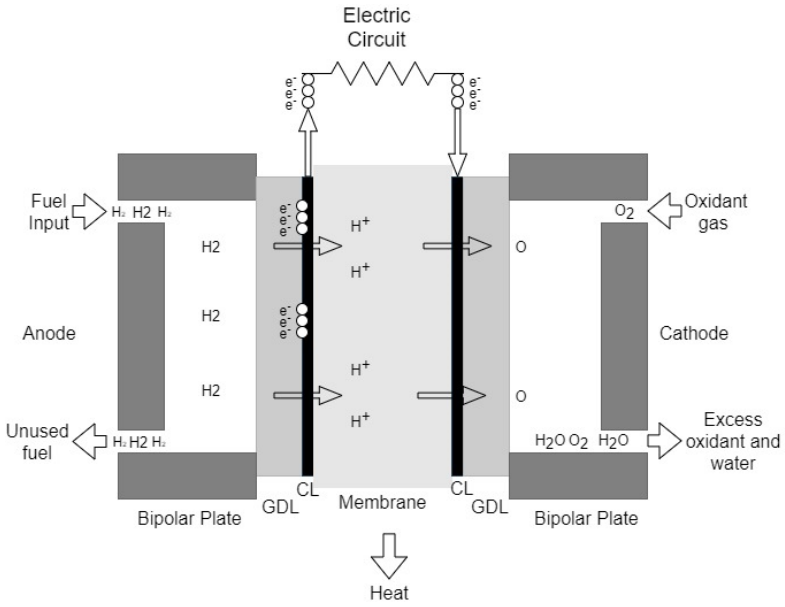


Figure 2.1. Operation of the PEMFC

In every chemical reaction some entropy is produced, so a portion of the $H_2$'s higher heating value cannot be converted into useful work electricity. Each charge must exceed an activation energy barrier (through the electrolyte, electrode and bipolar plate) to move within the PEMFC. The speed of electrochemical reactions in PEMFC depends on the rate of consumption and production of electrons. The size of the energy partition to come through is equal to the Gibbs free energy change between the product and reactant [5], [13]. Taking this into account, the potential energy of the cell which is equal to 1.23 V is calculated as follows:

$$E = \frac{-\Delta G}{nF} \tag{4}$$

The electrochemical reaction's which is a function of the Gibbs free energy, heterogeneous rate coefficient, k, can be calculated as below [13]:

$$k = \frac{k_B T}{h} \exp\left(\frac{-\Delta G}{RT}\right) \tag{5}$$

where $k_B$ is the Boltzmann's constant (1.38049 $10^{-23}$ J/K), T is temperature, h is Plank's constant (6.621 $10^{-34}$ Js), R is ideal gas constant (0.082 L.atm/mol.K) and $\Delta G$ is the Gibbs energy of activation (kJ/mol).

The Gibbs' free energy for electrochemical reactions can be admitted as consisting of both chemical and electrical terms. In this circumstance, for a reduction reaction:

$$\Delta G = \Delta G_{ch} + \alpha_{Rd} FE \tag{6}$$

For an oxidation reaction:

$$\Delta G = \Delta G_{ch} + \alpha_{Ox} FE \tag{7}$$

where $\Delta G_{ch}$ is the chemical component of the Gibbs free energy, F is the Faraday's constant, $\alpha$ is a transfer coefficient, and E is the potential. In the literature, there is a lot of confusion about the symbols because the symmetry factor $\beta$ is sometimes used instead of the transfer coefficient $\alpha$ [5].

## 2.2. Voltage Loss

PEMFC has some voltage losses, even when no external current is produced. The initial voltage loss is smaller for the cells operating at high temperatures, than low temperatures. In addition to this, HT-PEMFC exhibit more linear behavior. This potential after the first loss is called the open circuit voltage (OCV). The OCV is anticipated to decrease even more as a result of current being generated due to inevitable losses when the electrical closed circuit is connected with a load. These all losses named as polarization which means the difference between the electrode potential and the equilibrium potential [5]. There are four main voltage losses in the PEMFC.

### 2.2.1. Activation Polarization Loss

The activation loss is shown up in the low current region. Before the current and ionic flows are occurred, the electronic barrier region must be hurdled. The activation loss is directly proportionate to the increase in current flow [14]. Activation losses occur at both anode and cathode side; but $O_2$ reduction has slower reaction than $H_2$ oxidation because it requires higher over potentials. According to Butler- Volmer equation:

$$\text{Anode side: } \Delta V_{act,a} = E_a - E_{r,a} = \frac{RT}{\alpha_a F} \ln\left(\frac{i}{i_{0,a}}\right) \tag{8}$$

$$\text{Cathode side: } \Delta V_{act,c} = E_{r,c} - E_c = \frac{RT}{\alpha_c F} \ln\left(\frac{i}{i_{0,c}}\right) \tag{9}$$

Where $E_r$ is equilibrium or reversible potential, $E_a$ anode and $E_c$ cathode potential, i is net current:

$$i = nF\left\{k_{0,f} C_{Ox} \exp\left[\frac{-\alpha_{Rd} FE}{RT}\right] - k_{0,b} C_{Rd} \exp\left[\frac{\alpha_{Ox} FE}{RT}\right]\right\} \tag{10}$$

$i_0$ is exchange current density:

$$i_0 = nFk_{0,f}C_{Ox}\exp\left[\frac{-\alpha_{Rd}FE_r}{RT}\right] = nFk_{0,b}C_{Rd}\exp\left[\frac{\propto_{Ox}FE_r}{RT}\right] \quad (11)$$

### 2.2.2. Internal Currents and Crossover Losses

Although the polymer membranes are electrically insulating, some electrons may find a "short cut" through the membrane, causing less voltage to be generated. These losses may seem unimportant in the PEMFC operation, because the $H_2$ permeability or electron transition rate is less the $H_2$ consumption rate than produced or the generated total electric current. However, when the PEMFC operates at very low current densities or at an open circuit potential, these losses might have a huge effect on cell potential [5].

$$i = i_{ext} + i_{loss} \quad (12)$$

### 2.2.3. Ohmic (Resistive) Losses

Ohmic polarization is occurred from the resistance to the external electrical circuit, the transfer of ions in the electrolyte and the transfer of electrons through the electrodes. The major ohmic loss become in the electrolyte, which is decreasing by reducing electrode separation, increase the electrolyte's ionic conductivity by modification of the electrolyte qualities [14].

$$\Delta V_{ohm} = iR_i \quad (13)$$

where i is current density and $R_i$ is total internal resistance.

$$R_i = R_{i,c} + R_{i,i} + R_{i,e} \quad (14)$$

where $R_{i,c}$ is contact resistance, $R_{i,i}$ ionic resistance and $R_{i,e}$ electronic resistance.

### 2.2.4. Concentration Polarization

Concentration losses are evident in the high limiting currents in which gas reactive flow becomes more difficult to reach to the PEMFC reaction zones but occurs at all current density ranges. Since the reactant gas is consumed by the electrochemical reaction at the electrode, there will be a potential reduction due to the decrease in the initial concentration of the fluid mass in the medium.

This reduction causes a concentration gradient in the PEMFC. The slow diffusion of the gas phase in the electrode pores, the electrolyte solution of the reagents, the dissolution of the products from the system, and the diffusion of the reagents and products through the electrolyte from the reaction are responsible for the formation of concentration polarization [14].

$$\Delta V_{conc} = \frac{RT}{nF} \ln\left(\frac{i_L}{i_L - i}\right) \tag{15}$$

Where $i_L$ is limiting current density:

$$i_L = \frac{nFDC_B}{\delta} \tag{16}$$

Where $C_B$ is bulk concentration of reactant, $\delta$ is diffusion distance, D is diffusion coefficient of the reacting species.

Total cell voltage is:

$$V_{cell} = E_r - (\Delta V_{act} + \Delta V_{conc})_a - (\Delta V_{act} + \Delta V_{conc})_c - \Delta V_{ohm} \tag{17}$$

The polarization curve is generated by removing activation polarization losses, concentration polarization losses and ohmic losses from the equilibrium potential. The polarization curve is given in the Figure 2.2.

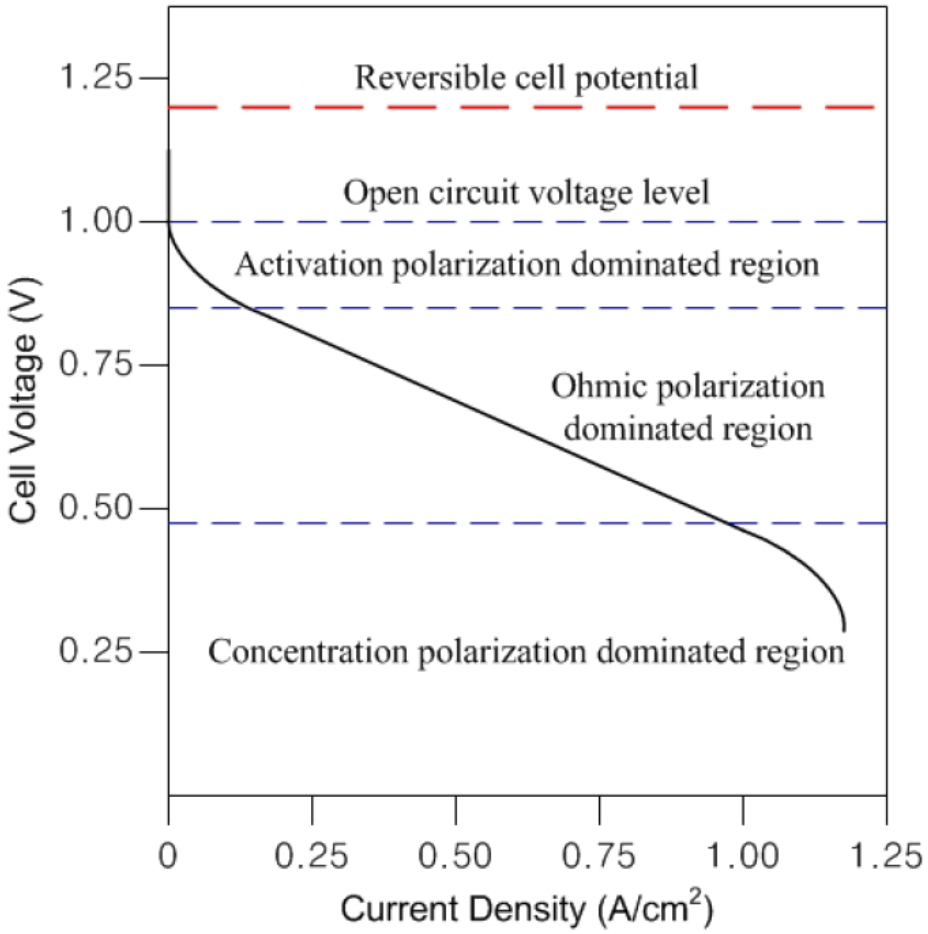


Figure 2.2. General polarization curve of the PEMFC [15]

### 2.3. Main Components of the PEMFC

PEMFC are generally composed of 5 main parts; MEA, bipolar plate, gasket, current collector and end plates.

#### 2.3.1. MEA

The MEAs, are composed of two different layers due to the Catalyst Layer (CL) location, are known as the heart of the PEMFC. In the first type of MEA, catalyst ink directly coated onto both sides of the membrane. This structure which is called Catalyst Coated Membrane (CCM) forms the three-layer MEA. In the second type MEA catalyst ink applying onto the Gas Diffusion Layer (GDL) leads to a basic two-layer structure [16]. This structure is called a Gas Diffusion Electrode (GDE). When

two GDEs are sandwiching with a membrane or the CCM are sandwiching with two GDL, they formed a five-layer MEA. The five layer MEA are shown in the Figure 2.3.

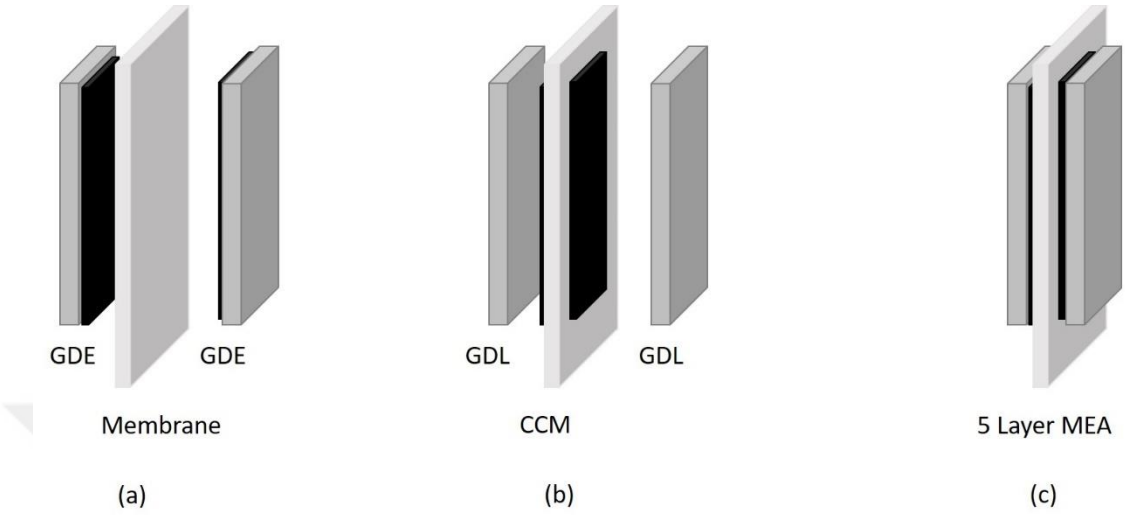


Figure 2.3. (a) MEA with GDEs and Membrane (b) MEA with GDLs and CCM (c) Five-layer MEA

#### 2.3.1.1. Membrane

Polymeric membranes have three main roles [17]:

(1) Charge carrier for protons

(2) Separation of reactive gases

(3) Electronic insulator to prohibit the electrons from transfer through the membrane.

In LT-PEMFC most preferred membrane is Nafion® which is developed by DuPont. Nafion® membrane is a type of perfluorocarbon sulfonic acid membrane. (Figure 2.4). This membrane is an excellent proton conductor which has excellent chemical stability, good mechanical strength, high ionic conductivity etc.

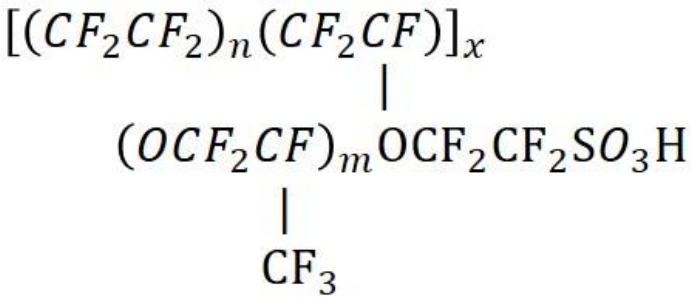

Figure 2.4. Chemical structure of Nafion® membranes, m=1,2 or 3;n=6,7; x=100[18]

However, the operation of these Nafion® membranes at temperatures above 100°C is adversely affected because the water required for the conductivity of the membranes evaporates. It is preferred that PEMFC works at high temperatures because of the problems such as catalyst poisoning (especially Pt and Pt alloy) caused by adsorbed CO decreases from 150 to 200°C [19].

On the other hand, Acid–base high temperature membranes such as poly(2,2-(m-phenylene)-5,5-bibenzimidazole (PBI)) membranes with doping some strong acids can easily work at higher working temperature [20]. PBI is an aromatic heterocyclic polymer and the chemical structure is shown in Figure 2.5.

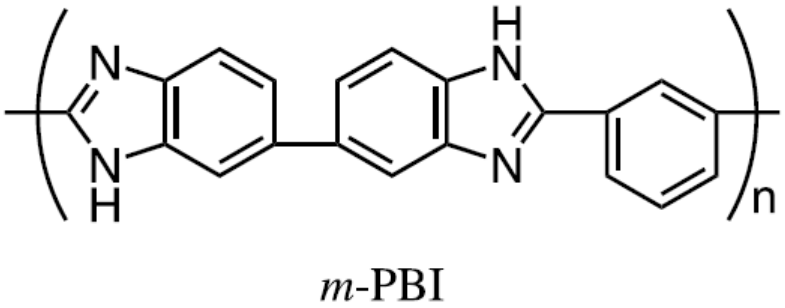


*m*-PBI

Figure 2.5.Chemical structure of PBI [21]

Their aromatic backbone supplies good chemical resistance, high thermal stability at 430°C that is a glass transition temperature and high mechanical endurance. It is necessary to obtain the minimum proton conductivity (> 0.05 $S \cdot cm^{-1}$) required to operate the fuel cells, but, PBI do not have enough proton conductivity without acid

doping because the internal conductivity is very low (about 10 -12 S/cm) [22]. The proton conductivity of fully doped PBI membranes at 200°C (0.07 S/cm) is higher than fully hydrated perfluorinated membranes, which require almost continuous humidification [23].

PBI membranes conduction properties depend on the phosphoric acid ($H_3PO_4$) doping level and water content. High doping levels increase the proton conductivity, but the mechanical properties of the acid-doped membranes decrease. $H_3PO_4$ doping of PBI from an aqueous solution takes place through the coordinating (imide) sites of the polymer but at the molecular level, acid addition can be a very complex process. Many variables can change according to the acid loading level [24]. Chemical structure of a $H_3PO_4$ doped PBI is shown in the Figure 2.6.

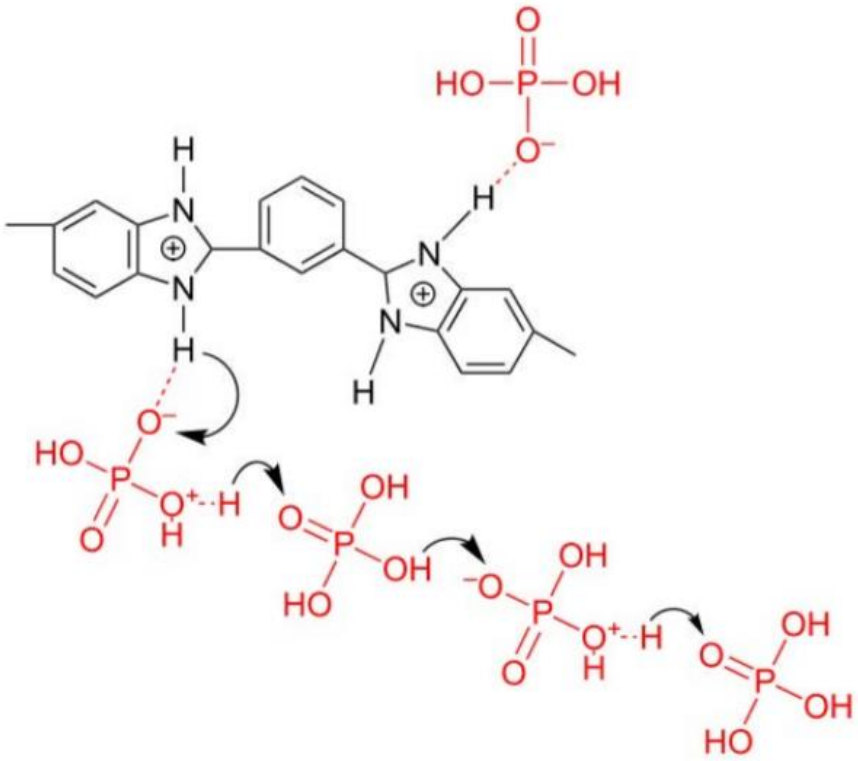

Figure 2.6.Proton conduction mechanism of $H_3PO_4$ doped PBI membrane [25]

### 2.3.1.2. Catalyst layer

Catalysts are the electrodes which are used for $H_2$ oxidation and $O_2$ reduction reactions at the anode and cathode side of the PEMFC [26]. The main roles of the catalyst are:

(a) Ensure active area for reaction

(b) Meet conductive route of both proton and electron

(c) Include the pores which allow water and reactant gas transfer

(d) Contain the active triple phase boundaries where all the reactants can get mixed

(e) Operation is chemically stable under pH and voltage conditions

(f) Tolerable to reactant composition

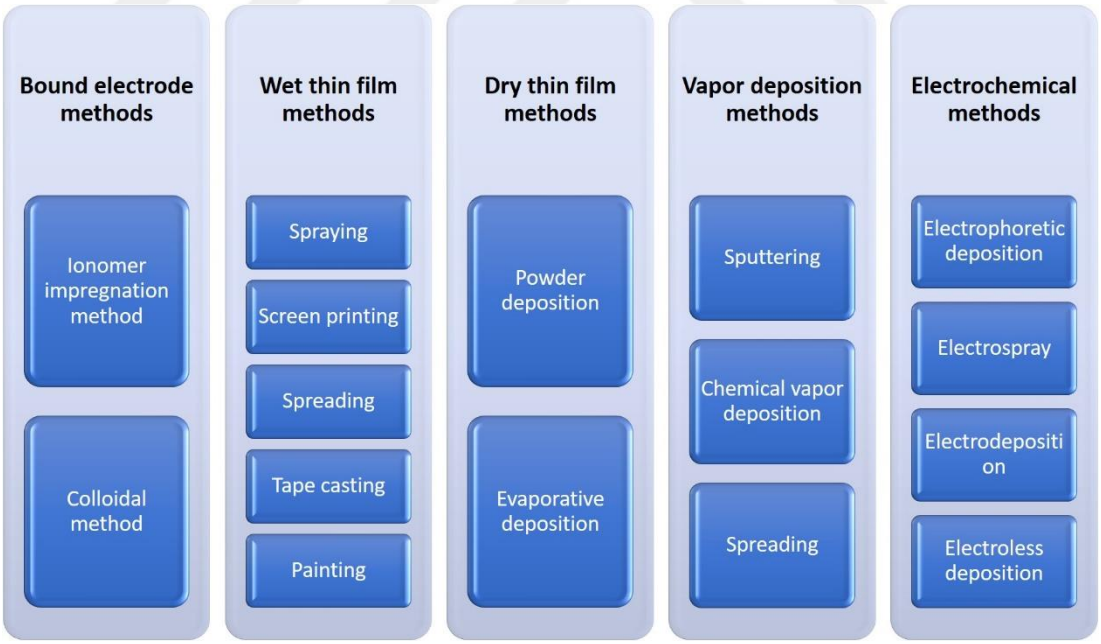


Figure 2.7. Catalyst layer fabrication methods

In the literature, there are several methods to fabrication of catalyst layer as shown in the Figure 2.7. The decal, painting, screen-printing, spraying methods are most preferred techniques. However, in the preparation of fuel cell CCMs or GDEs, ultrasonic, sonochemical and sonoelectrochemical methods which are advantageous compared to other methods are preferred depending on the unusual experimental conditions occasioned by cavitation, water sonolysis and the phenomenon of advanced mass transport [27].

The ultrasonic spraying system is preferred because it bounces back onto the substrate and causes a solution to problems such as over-spraying of liquid, clogging problems at the nipple and agglomeration of nanoparticles in solution [28].

#### 2.3.1.3. GDL

A suitable GDL for fuel cells is expected to have the following characteristics:

(a) Relative stability in the fuel cell environment

(b) Elastic property under compression

(c) High permeability for gases and liquids

(d) Good electrical conductivity

GDLs are usually divided into two main types: carbon paper or carbon fabric. Although these varieties are similar to the usage area, they have different advantages and disadvantages due to their structure properties which can significantly affect the transportation of heat, current, reactant gas and water. These GDLs are generally composed of porous composites. For this reason, improving the hydrophobicity properties include binder such as polytetrafluoroethylene (PTFE) and carbon-based material to improve the electrical conductivity properties. Moreover, these added materials positively affect the durability problems of GDLs [29].

### 2.3.2. Bipolar Plates

Bipolar plates are produced to carry out many functions [30]. These functions are:

(a) Distribution the fuel and oxidant within the cell

(b) Preventing leakage of reactants and coolant

(c) Facilitating water management within the cell

(d) Remove the current from the cell

(e) Separating stack into cells

(f) Make easier the heat management of fuel

In order to reduce the cost of fuel cells, cells can be connected in series by means of bipolar plates. In this way, the cathode of a cell is attached to the anode of the contiguous cell [8]. To decrease the cost and weight of the bipolar plate of PEMFC, bipolar plates are also manufacturing with different type of materials. This materials must meet the following conditions to be used efficiently [30]–[33]:

ı. Electric conductivity > 100 S/cm to decrease ohmic losses in the fuel cell.

ıı. Interface contact resistance (ICR) < 30 mUcm$^2$

ııı. $H_2$ and $O_2$ permeability < $2\times10^{-6}$ cm$^3$/cm$^2$.s to decrease power losses resulting from fuel cross-over.

ıv. Chemical stability in the slightly acidic water pH < 4

v. Corrosion rate < 16 μA/cm$^2$

vı. Compressive strength > 151.7 kPa

vii. Flexural strength >59 MPa

viii. Impact strength >40.5 $Jm^{-1}$

ix. Thermal conductivity >10 $W(mK)^{-1}$

x. Density < 5 $gm/cm^2$

Main materials studied to produce bipolar plates are graphite and sheet metal (coated and uncoated). Graphite is generally chosen for fuel cell bipolar plates according to its high conductivity, chemical compatibility and corrosion resistance. The high density graphite plates manufacture is a complicate process which involves high-temperature process that can occasion defects in the material such as cracks and porosity. After heat process, the material must be processed with certain resins to decrease its porosity, which causes reduce in its electrical conductivity. Besides, an enhancive factor the cost of the graphite plates is the fact that they are brittle and inclined to damage during manufacturing and handling. Due to these properties, a thicker material must be selected to be able to withstand the stresses and the tightening torque in the fuel cell. This also decreases the power density of the fuel cell in terms of $kW/m^3$ [2], [30].

The main reasons for the use of metallic bipolar plates instead of graphite plates are the high material and processing costs of the graphite plates and the need for high volume coating to block the small pores despite the use of high density graphite due to their porous structure. However, the metallic bipolar plate materials need to be improved to withstand the corrosive. This can be accomplished by surface treatment, such as by alloying, chemically or by coating with a metallic or non-metallic compound [2]. But in both methods, the cost of production of metallic bipolar plates is increasing.

During a PEMFC operation, corrosion can materialize both at the anode and cathode. At the anode side, the existence of a reducing environment can decrease the protective metal oxide layer thus cause the undesirable hydride formation and metal

dissolution in the water. This problem is increased with the addition of water vapor to the supply fuel stream. Because of this problem, PEMFC contamination and the catalyst layer activity are affected negatively. At the cathode side, the corrosion rate of metallic bipolar plates can substantially increase with the presence of oxidizing environment, cause to performance losses and even early failure of the whole stack [32].

Composite bipolar plates are used as an alternative to bipolar plate types. They can be separated as metal or carbon based. Composite bipolar plates associated porous graphite, polycarbonate plastic and stainless steel in a strive to develop the advantage of the different materials. Porous graphite plates can be used for sealing by stainless steel and polycarbonate parts, because the production of these plates is not as expensive or time consuming as the production of non-porous graphite plates. Carbon-based composite bipolar plates can be used differently in fuel cells. Carbon composite bipolar plates, thermoplastic (polypropylene, poly (vinylidene fluoride), polyethylene) or thermoset resins (epoxies, phenolics, and vinyl esters) are made without fiber reinforced and with fillers. Examples of the bipolar plate is shown in the Figure 2.8.

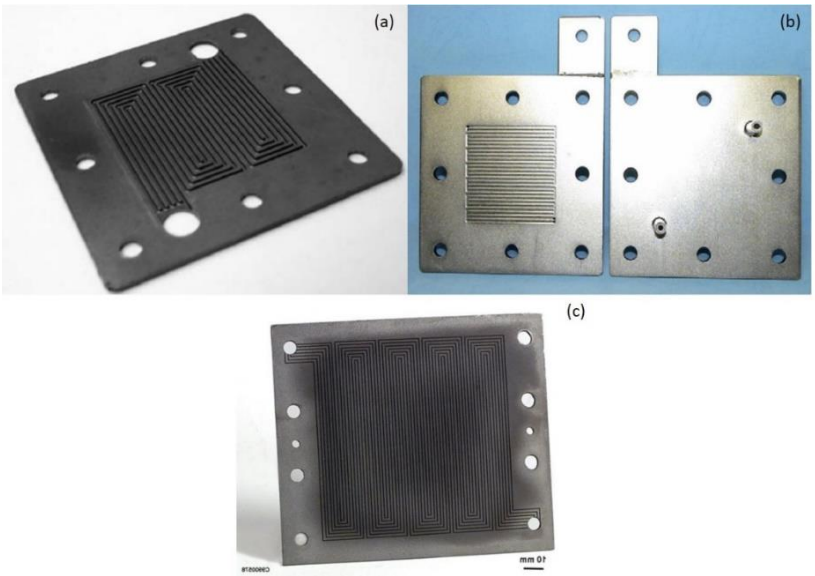


Figure 2.8.Bipolar plate types (a) graphite bipolar plate (b) metallic bipolar plate (c) composite bipolar plate [34]–[36]

After manufacturing the bipolar plates at high temperature and pressure, the gas flow channels are machined, with different configurations. The flow channels have two main tasks:

(a) The gases are distributed over the surface of the membrane with the help of these channels.

(b) They are connected with individual fuel cells in series to form a fuel cell stack and work as electrodes that remove the electrons from anode to cathode to produce required voltage output.

The design of flow channels is very important for uniform distribution of reactive gases. If a uniform flow distribution is not achieved, the usage of catalyst and energy efficiency are reduced. In addition, uneven distribution of current density decreases cell life [16], [37]. Figure 2.9 and Figure 2.10 shows some traditional bipolar plate flow field which are usually used in PEMFCs.

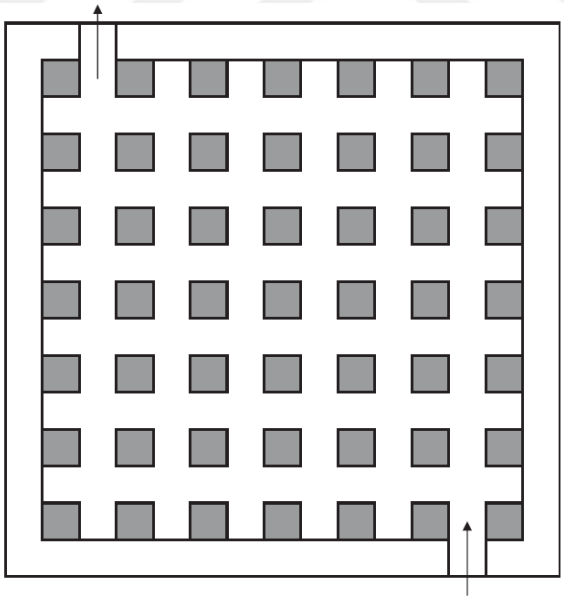

Figure 2.9. Pin-type flow-field [37]

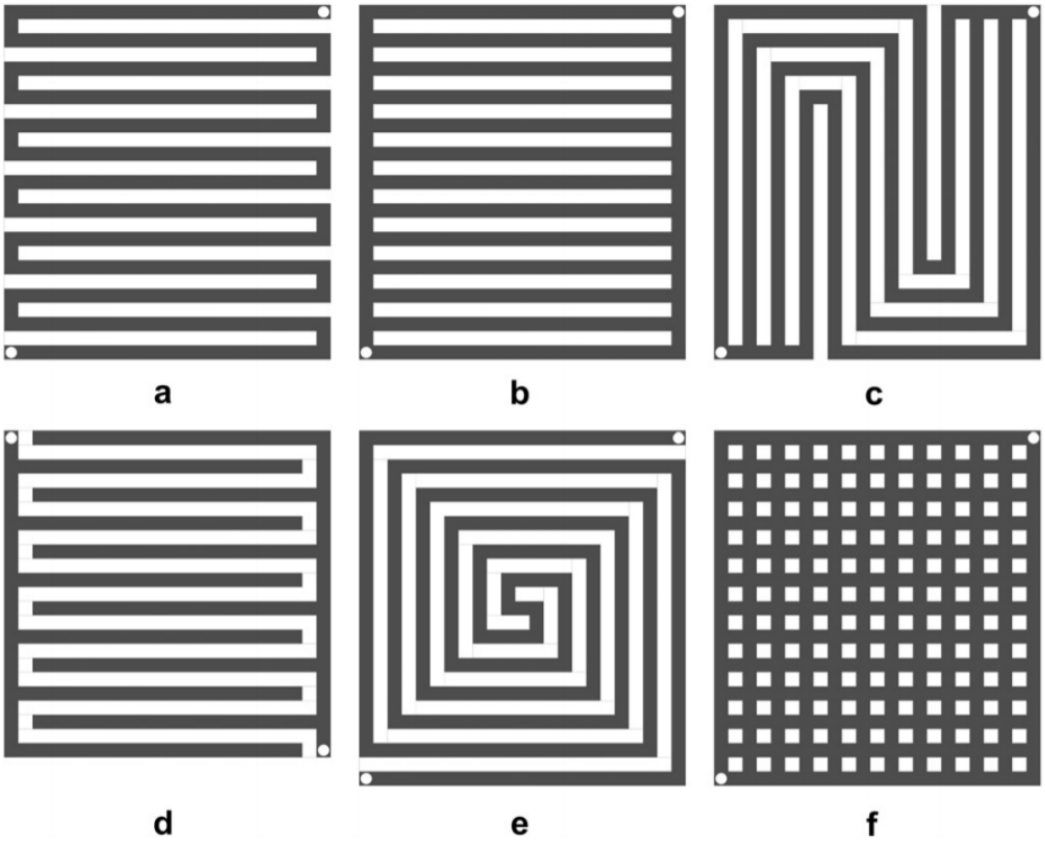


Figure 2.10. Schematic of various flow field patterns for PEMFC: (a) Serpentine; (b) Parallel; (c) Parallel serpentine; (d) Interdigitated; (e) Spiral; (f) Porous mesh [38].

### 2.3.3. Gaskets

The gaskets are inserted between bipolar plates and the MEA in PEMFC. The main roles of gaskets are to avoid the leakage of reactant gases and coolants from the flow channels into the cell. Also, they work as electrical insulators between the bipolar plates and MEA and ensure stack height control. Generally, polymeric materials are used as gaskets [8].

### 2.3.4. End Plates

End plate is an important component for PEMFC. The main reasons to use end plate are given in below:

(a) Stacking of various other components of stack (five -layer MEA, bipolar plate, gasket, current collector) to be a stack

(b) Provide flow channel to inlet the stack for reactant gases and coolant fluid

(c) Enable good sealing at several interfaces.

(d) Apply a pressure equal to the entire fuel cell to reduce ohmic resistance. If pressure is applied uneven, proper electrical connection cannot be achieved and voltage drop occurs in the cell.

End plates are compressed with a certain force from the edges for smooth pressure formation. This compression force is called a clamping force. The clamping force is equal to the force needed to compress stack and internal forces. The assembly pressure impresses the feature of the contact interfaces between components for thin dimensions and the fuel cell layers' low mechanical strength of against the gaskets, bipolar plates, and end plates. If insufficient or non-uniform clamping force is used, there will be some problems, such as fuel leakage, internal combustion, and high contact resistance. Also, high clamping force can damage the stack, resulting in a weathered porous structure and a choke of the gas diffusion layer. Thus, it will reduce the cell performance as well as increase the degradation. Every stack has a proper clamping force depending on the fuel cell materials and stack design [39].

### 2.4. Single cell, Stack and Systems

A single fuel cell has one MEA, so they have only an anode and a cathode. According to voltage losses, the maximum voltage of the cell is 1 V. During the operation, the voltage is even less because of the generated current [16]. In LT-PEMFC normally operated at least 1 $A/cm^2$ at 0.6 V operation voltage but this value is decrease in HT-PEMFC. A single cell consists of two end plate, two current collectors, two bipolar plate, two gasket, two gas diffusion layer and a MEA, as shown in the Figure 2.11. In single cell tests, generally end plates does not using so heating is realized by two pairs of heat tape pieces which are stick onto the copper

current collector plates. This heating tapes allows the cell to operate at temperatures up to 120 ° C, but at higher temperatures the heating of HT-PEMFC should be provided with the heating plate.

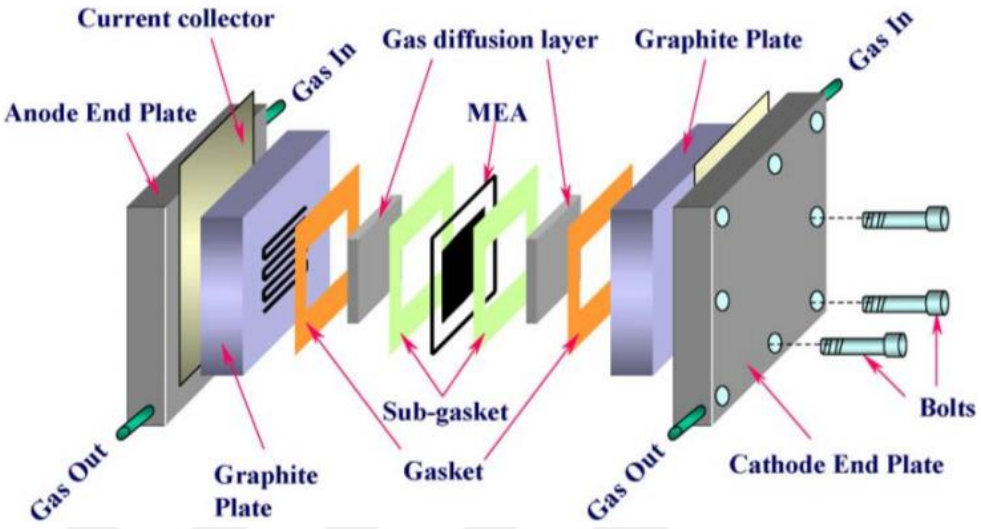


Figure 2.11. A single PEMFC [40]

The voltage of single PEMFC remains very low for required applications. More than one cell must be connected to produce enough voltage. This connection can be made in series and/or in parallel reactant and oxidant feeding. When the gas supply to the stack is carried out in parallel, the gas to all cells is provided in parallel from reactant/oxidant inlet. When the gas supply takes place in series, outlet of the first cell enters the second cell, outlet of the second gas enters the third and so on. The series gas supply pattern helps to prevent the same gas distribution between cells, but to keep away from a large pressure drop, this gas supply method can only be used for masses with a small number of fuel cells [16]. The parallel gas flow configurations can be the parallel flow which the inlet gas flow direction is same with the outlet gas flow direction or reverse flow which the inlet gas flow direction is opposite with the outlet gas flow direction [41]. Gas supply methods are shown in Figure 2.12.

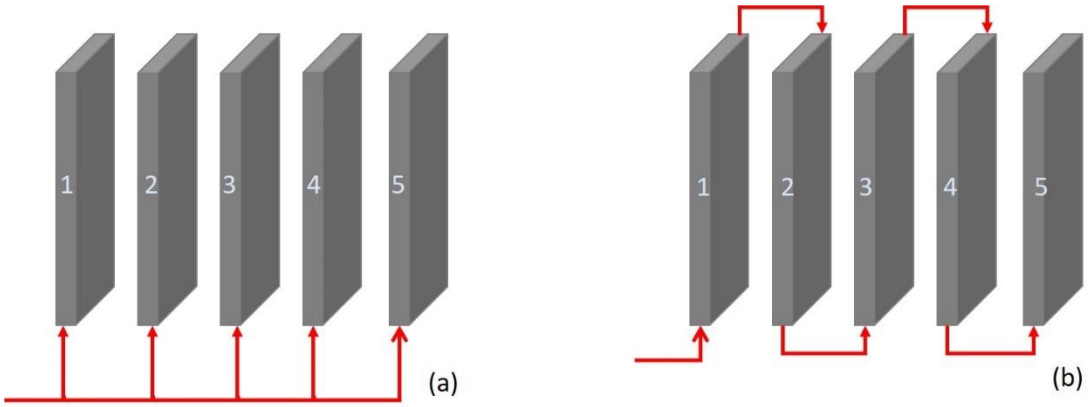


Figure 2.12. (a) Parallel gas flow configuration (b) Serial gas flow configuration of five cells

The PEMFC stacks are designed using current collectors so that one side of the stack is the anode and the other side is a cathode. In this way, serial electrical connection between the cells occurs. The potential power generated by a series of PEMFC stacks connected in series depends on the active area of the cells that make up the stack and the number of fuel cells [16]. The PEMFC stack and the position of the single cell in the stack are shown in the Figure 2.13.

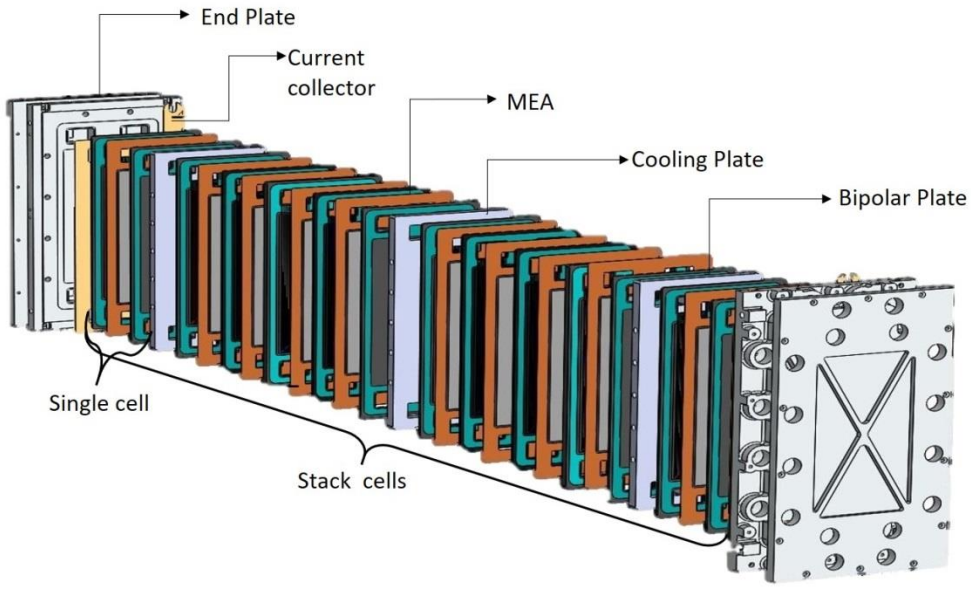


Figure 2.13. Fuel cell stack

In addition to PEMFC stacks Balance of Plant (BoP) equipment must be used to operate fuel cell systems. Examples of such equipment include compressors, valves, control equipment, heaters.

### 2.5. Cooling Methods

The choice of cooling system is another affecting factor of performance in PEMFC. The stack is cooled to operate temperature to protect the PEMFC components from excessive heat, keep the cell temperature constant, and heat transfer for μCHP. Cooling system are separated two different types of inside the stack; cooling with air and liquid [41]. Examples of the cooling ways of these two main types is given in Figure 2.14.

The air-cooling system, that uses ambient air to remove heat generated by the stack, can be carried out in three ways. These are cooling plate, cathode air and heat spreader [42]. In the cathode air cooling method, the stack volume is increased because of the stack area must be larger than the cell active area is used. In the cooling plate method, which is generally used for stacks that produce more than a few hundred watts of power, separate air plates are used [43]. In heat spreaders cooling method, heat is transferred from central region of PEMFC to the edges of the stack, then the heat is removed with conduction [42]. The use of air-cooling systems in HT-PEMFCs causes some disadvantages such as a decrease in heat flux and an increase in heat exchanger size.

The other method, liquid cooling operated with cooling plates placed in the stack are divided into three types; water, oil and evaporative cooling. In liquid cooling system, a liquid is pumped from the cooling channels which is placed into the stack. Then the heat is transferred from the stack with the helped of heat exchanger effect in liquid cooling system but in evaporative cooling method caused membranes phosphoric acid loss for HT-PEMFC. In water cooling method, water has high heat capacity, but the water must be deionized and can be caused corrosion inside the PEMFC. [44], [45].

Thermo-oil which is used in oil cooling methods, has many advantages because of its high heat capacity. For example, since the boiling point of the cooling oils is higher than working temperature of HT-PEMFC, there are no phase change occurs inside the cell [46].

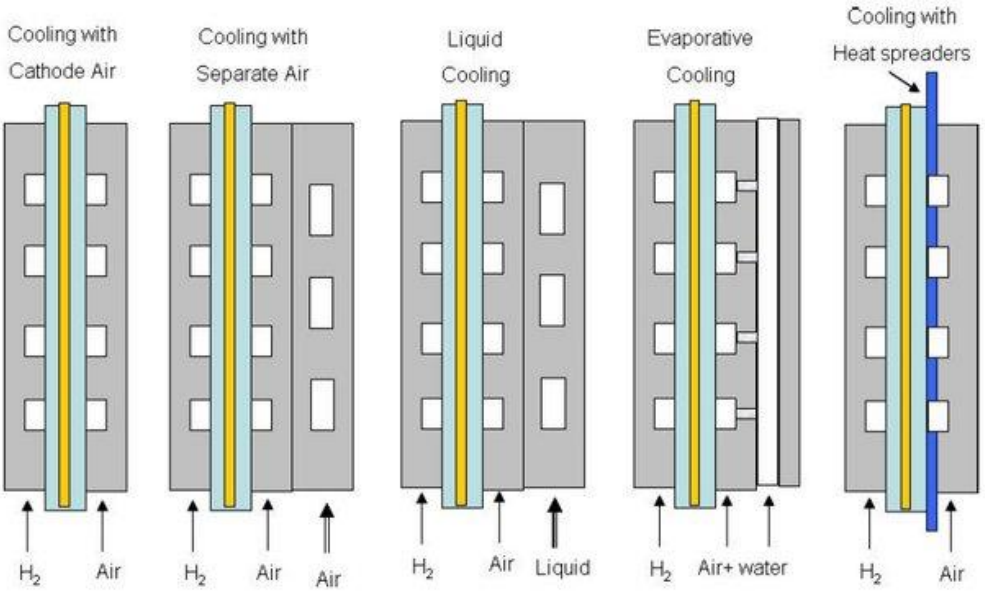


Figure 2.14.Cooling Methods [43]

## 2.6. HT-PEMFC

PEMFC have some problems that need to be solved before they are completely commercialized. For example, improper liquid water generation, heat management, slow electrochemical cathode kinetics, $H_2$ supply and high cost [44]. Usage of the HT-PEMFC can overcome these problems.

Due to the HT-PEMFC working on the boiling temperature of water, the water in the catalyst layer of the fuel cell is only present in the vapor phase. Thus, water is easily transported in the membrane, electrodes and GDL. In this way, the structure of the GDE and the flow area design of the bipolar plate have a reduced effect on cell performance. One of the best advantages is the generated heat when it produces can be used for other applications (e.g. μCHP) and this application increases system efficiency crucially [45].

Pure $H_2$ is preferred as a fuel in PEMFC systems because of their high efficiency and zero emissions, but their production, handling and storage still cause difficulties in the commercialization of PEMFC systems [46], [47]. One of best solutions to the $H_2$ supply is the usage of the HT-PEMFC systems with reformer systems which is used to the produced reformate gas mixture. The reformate gas mixture can be produced by inexpensive industrial processes with using natural gas or methane. Thus, the commercialization of PEMFCs accelerates and facilitates their use in daily life. The reformate combined PEMFC systems can be used in movable and small stationary applications [52]. However, some pollution such as $CO_2$, CO, $CH_4$ and $N_2$ and $NH_3$ can be found in the $H_2$ produced in this way. Generally used reformers produce $H_2$ rich reformate gas mixture containing 40-70 % $H_2$, 15-25 % $CO_2$ and 1-3 % CO. CO adsorption of HT-PEMFCs decreases and CO electro-oxidation of $CO_2$ on the catalyst surface increases with increasing temperature [48]–[51]. Also, LT-PEMFC cannot be used due to low tolerance of these impurities so HT-PEMFC is preferred for this type of applications [47]–[49].

Previous studies in the literature are shown in the Table 2.1. Jannelli et al. compare Nafion, PBI and Aromatic polyethers-pyridine. PBI membrane-based stacks operated at 160$^o$C and aromatic polyethers-pyridine membrane-based stacks operated 180$^o$C. The stacks fed with reformate gas mixture which is include $H_2$, $N_2$, $CO_2$, $CH_4$. When they compare the membranes two situation which were fixed current density and cell voltage the maximum power for fixed current and minimum cell number for fixed cell voltage is obtained from Nafion membrane. When their system integrated with reforming unit (RFU) both HT-PEMFC electrical power increase 2.52 kW and total efficiencies of the systems are 79 % and 78 % of aromatic polyethers-pyridine membrane based stacks and PBI membrane based stacks, respectively [49]. Weng et al. compared the performances of 4,7 and 9 cells which are produced maximum powers 35,65, 90 W respectively. They also made thermal balance analysis for the stacks. Analysis show that the HT-PEMFC stacks need one cooling channel for three or four bipolar plates, unlike a LT-PEMFC stack with a cooling channel in every bipolar plate [52]. Authayanun and Hacker designed a trigeneration system with using HT-PEMFC with methane, $CO_2$, $H_2O$, $H_2$ and CO. They were tested

stoichiometric ratios at anode and cathode side, temperature and pressure effect. Their study shows that when anode side stoichiometry increases electrical efficiency decrease and energy efficiency increase, and they preferred 4 as cathode stoichiometric ratio for efficiency. In addition, with the increasing temperature, both electricity and energy efficiency increased, with the increase in pressure, energy efficiency increased but electrical efficiency decreased [53].

There are very few studies in the literature about the HT-PEMFC stack, and most of the studies about the high-power stack. In this study, HT-PEMFC with 300 W net power working with reformed gases is designed and manufactured. In the literature, the effect of CO on the performance of HT-PEMFC was studied with 1-5 vol. % CO and observed more the than 3 % CO constructions significantly affect the performance of the fuel cell. Based on the literature it was decided to use the ideal reformate gas mixture concentrations as 75 vol. % $H_2$, 22 vol. % $CO_2$ and 3 vol. % CO [54]. Micro cogeneration study was carried out with HT-PEMFC stack which has a unique cooling system and also the electrical and thermal efficiency values of the system were determined.

Table 2.1.Previous HT-PEMFC stack researches

| Active area ($cm^2$) | Membrane | Cell number | Power (W) | Temperature ($^oC$) | Anode Reactant gas (% vol.) | Ref |
|---|---|---|---|---|---|---|
| 200 | PBI / Aromatic polyethers pyridine | 46 | 1210<br>1140 | 160<br>180 | Reformate (75 $H_2$/19.87 $CO_2$/2.82 $N_2$/ 2.38 $CH_4$ and <0.55 ppm CO) | [49] |
| 31.4 | Advent TPS® | 4/7/9 | 35/65/90 | 160 | $H_2$ | [52] |
| 300 | PBI | 250 | 5000 | 160 | Reformate (70 $H_2$/0.04 $CH_4$/1.58 CO /28.30 $CO_2$) | [53] |
| 45 | Celtec P®-1000 | 30 | 400 | 150 | $H_2$ | [55] |
| 50 | PBI | 100 | 1000 | 160 | Reformate (77.62 $H_2$/0.65 CO/1.65 $CH_4$/19.86 $CO_2$) | [56] |

Table 2.1. Continued

| Active area ($cm^2$) | Membrane | Cell number | Power (W) | Temperature ($^oC$) | Anode Reactant gas (% vol.) | Ref |
|---|---|---|---|---|---|---|
| 100 | PBI | 40 | 1000 | 200 | $H_2$ | [57] |
| 165 | PBI | 55 | 2000 | 180 | $H_2$ | [58] |
| 300 | PBI | 135 | 5000 | 165 | Reformate (78.33 $H_2$/0.85 CO/19.11 $CO_2$/1.71 $CH_4$) | [59] |
| 81.28 | Celtec®-P 1100 | 40 | 658 | 120-180 | $H_2$ | [60] |
| 150 | Nafion/Zirconia | 80 | 3250 | 120 | $H_2$ /Reformate (70 $H_2$/30 $CO_2$ and 100 ppm CO) | [61] |
| 150 | PBI | 12 | 468 | 160 | $H_2$ /Reformate (75 $H_2$/22 $CO_2$/3 CO) | This Study |

# CHAPTER 3

# 3. EXPERIMENTAL STUDIES

## 3.1. Materials

The MEA was prepared by 3,3'-Diaminobenzidine (DAB), terephthalic acid (TPA), polyphosphoric acid (PPA) (115 % phosphoric acid equivalent), N-N dimethylacetamide ($CH_3C(O)N(CH_3)_2$ DMAc), phosphoric acid ($H_3PO_4$, 85 %), 70 wt. % Pt/C catalyst (Tanaka, Japan), carbon paper (Freudenberg H2315, Germany), and the necessary chemicals were purchased from Sigma Aldrich (USA). All the chemicals were used as in without further purification because they have analytical reagent grades and Millipore water was used wherever required. All gases having high purity (>99.98 %) used in the experiment were purchased from Linde.

In this study, polyvinylidene difluoride (PVDF) used as binder. The selection of the binder material used in catalyst layer that is one of the important factors affects the performance of the HT-PEMFC. The chosen binder material affects the mechanical properties of catalyst, gas permeability, utilization of Pt, the impregnation of $H_3PO_4$, and $O_2$ oxidation reaction rate (ORR) of the HT-PEMFC [62]. PVDF structures is hydrophobic. By using this material on the electrodes, the water formed on the cathode side in the cell let easily remove out the electrode and additionally the acid formation on the membrane is prevented by this hydrophobic structure. PVDF binder provided good impact and compressive strength, along improved wear resistance and higher thermal conductivity. Also, the cost of PVDF is comparatively low cost than other binder and has easy processing features.

Composite bipolar plates were selected to construct stack in the scope of this thesis because of its flexibility and conformity to assemble with other components of stack, such as gaskets, cooling systems, fittings, end-plates. Additionally, composite bipolar plates have important features concerning fuel cell manufacturing and environment such as corrosion resistance, low processing cost, flow channels that may be processed by molding (compression or injection) comparing with metal plate processing and pure graphite [63], [64]. The used composite bipolar plates were purchased from POCO Graphite. The properties of the composite bipolar plate are given in Table 3.1.

Table 3.1. POCO composite bipolar plate properties [36], [65]

| Properties | Values |
|---|---|
| Bulk Density | 680 S/cm |
| Surface Resistivity | 8 Ω/cm |
| Corrosion Rate | 80 μA/cm$^2$ |
| Apparent density | 1.78 g/cc |
| Flexural strengh | 89.63 MPa |
| Compressive strength | 151.68 MPa |
| Electrical resistivity | 1473.20 μΩ-cm |

The geometry of gas distribution channels on bipolar plates was designed and manufactured as multiple parallel serpentine type in three blocks. These flow channels were connected in series with a continuous flow channel from the input of manifold at gas supply channel one end to the outlet on the other end to collect exhaust gasses and reaction water. Since these channels have a long reactant flow channel, it may generate high pressure drop between inlet and outlet points. These pressure drop could create high flow rates and facilitate the removal of blockages in the cell. This allows the fuel cell to operate at high current densities [66].

The end plates were constructed by alloy of Aluminum in this thesis, because the this alloy is easy to manufacture and has higher strength than other metals [67]. The

surfaces of the end plates were coated with an eloxal (anodized) coating that is a dense oxide layer to make metal surfaces a harder and corrosion resistant. Connectors which were used to combine the stack were manufactured by stainless steel. Current collectors were manufactures by copper and then coated by Gold. The coating of Gold was preferred to increase the electrical conductivity and corrosion resistance of substrate material. Because the resistance to temperature and chemicals is higher than the other elastomers, gasket was selected as Viton®. It has also good resistivity and suitability to most lubricant, fuel, hydraulic fluids, wide range of corrosive chemicals and chlorinated solvents [8].

## 3.2. MEA Preparation

### 3.2.1. Membrane Preparation

The first step for manufacturing of PBI membrane was the synthesizing of PBI polymer. The PBI polymer was synthesized by solution polymerization method in our laboratory regarding to a procedure described by previous works conducted by our team [68]. The synthesis was carried out under the flow of nitrogen at 200°C for 18 hours in experimental setup which consisted a four-neck glass bottle, heating mantle, mechanical stirrer, calcium chloride ($CaCl_2$) drying tube and nitrogen inlet.

After PBI were synthesized, 5 wt. % PBI polymers were dissolved in DMAc at 60ºC. For single cell test, the solution was cast onto glass plate but for HT-PEMFC stack the 150 $cm^2$ membranes were coated by automatic film coater device. The prepared PBI based polymer solution was poured onto the film casting apparatus. The thickness was automatically spread on the glass plate on the casting apparatus with the help of a knife set by the micrometer. Then, the glass plates were placed in an oven at 80ºC for 12 h and then the solvent was evaporated by drying at 130ºC for 12 h. The dried membrane was washed by Milli-Q water to remove trace solvent. The thickness of the membranes was around 50 ± 5 μm. Preparation of the membrane for the stack is given in Figure 3.1.

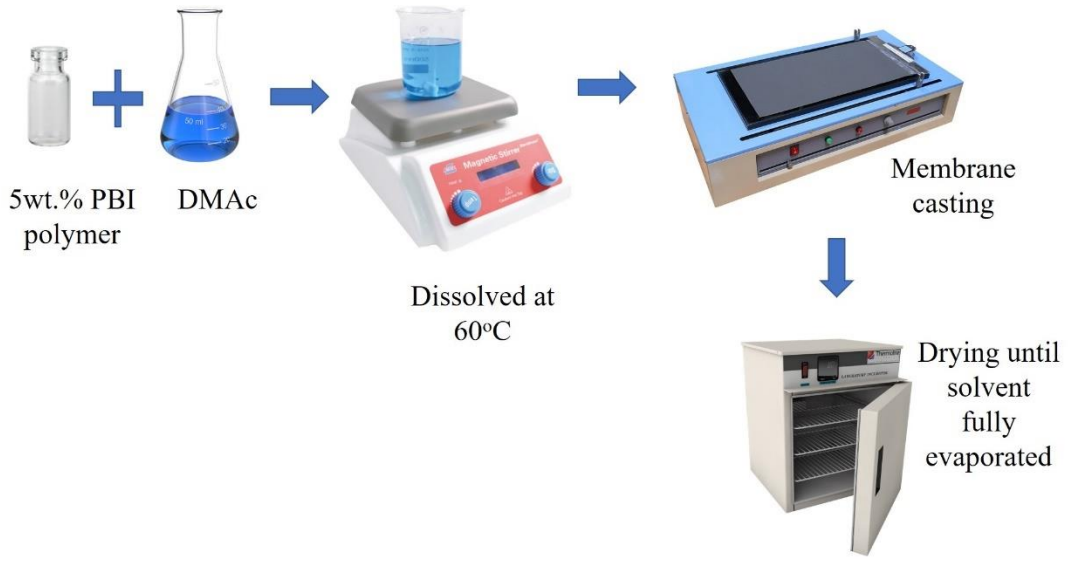


Figure 3.1. Membrane Preparation

The membranes were weighed before immersing in acid to measure the amount of doping. Then, the PBI was carried out immersing in the $H_3PO_4$ at room temperature for one-week $H_3PO_4$ doping. After a week, the membranes were removed from the $H_3PO_4$ solution and wiped the excess acid solution with a tissue before weighing. To calculate both acid and water based weight gain, the weight of the membranes were measured after loading and compared with the weight before doping [20].

Although the weight gain was caused by both phosphoric acid and water, it was assumed that the water uptake in the membranes do not change in the presence and absence of $H_3PO_4$. To calculate the acid retention capacity, the acid leaching tests were performed as described in previous study [20]: the membranes were kept in water vapor and the weight loss due to $H_3PO_4$ loss was determined for five hours by weighing the membranes every hour. The acid doping level and acid loss percentage equations are given in APPENDIX A.

### 3.2.2. GDE Preparation

The ultrasonic coating technique were used for manufacturing of GDEs that would be component of PBI MEAs tested within the scope of the thesis. The electrodes with

a highly homogeneous distribution of catalyst were prepared with the minimal loss by the ultrasonic coating technique [27].

The HT-PEMFC catalyst ink was prepared by using the method as described by Devrim [69]. Catalyst ink includes of 70 wt. % Pt/C, 5 wt. % PBI solution, DMAc and PVDF. The mixture was mixed in the ultrasonic mixer for 40 minutes before being charged to the ultrasonic sprayer. This solution was ultrasonically sprayed on commercial carbon papers by ultrasonic spray coater produced by the company of Sono-Tek with the model ExactaCoat using 120 kHz Impact Nozzle (Figure 3.2) by keeping GDL substrate on heated plate at 80ºC. The coating process was programmed with regard to the coating area and was carried out by full computer control. The catalyst ink was filled up in a syringe pump prior to atomization at the nozzle and sprayed onto the GDLs to produced 1 mg/cm$^2$ catalyst loading by leveling to a flow rate up to 0.5 mL/min.

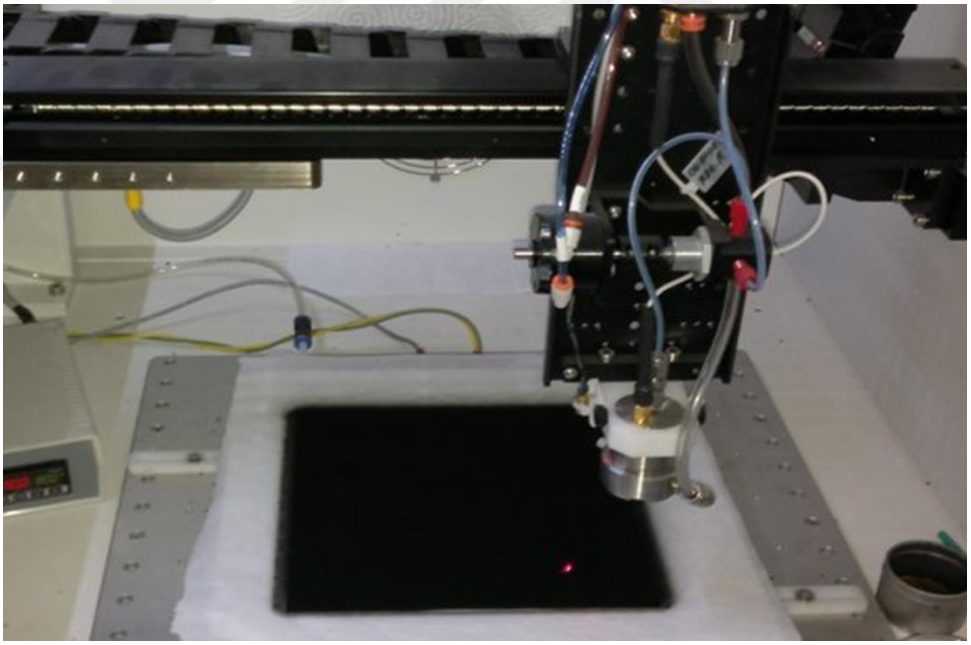

Figure 3.2 GDL coating process

Finally, GDLs were pressed onto the $H_3PO_4$ doped PBI membrane at 150 °C and 172 N/cm$^2$ for 10 minutes by hot press in Atılım University Hydrogen Energy and Fuel Cell Research Laboratory (Figure 3.3).

Figure 3.3. Hot press

### 3.3. HT-PEMFC Test System

The test station using in our laboratory was improved for the reformate gas mixture usage. The station equipped with a reactant gas supply unit, electronic load (BK Precision, USA) and test station software computer were used for performance test of the HT-PEMFC stack as shown in Figure 3.4. The current and voltage of the cells were monitored and computerize during the operation by the test station control and data acquisition software.

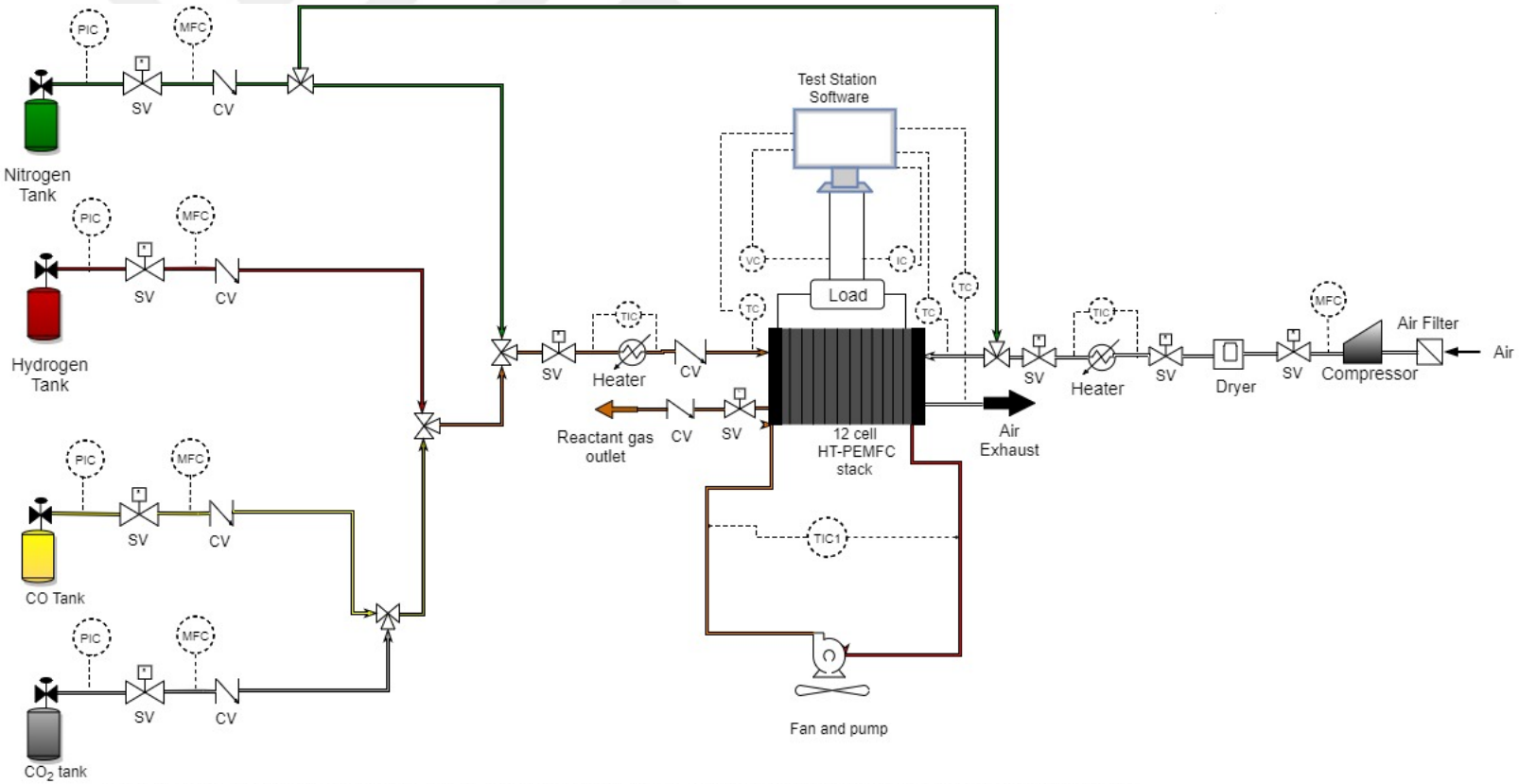


Figure 3.4.HT-PEMFC test system

Anode side gas streams from high-pressure tanks were controlled through the pressure, temperature, mass flow controllers (MFC), valves and heaters before entering the HT-PEMFC. The air at cathode side was supplied by an air compressor in that inlet-air was filtered. After the compressor, an additional dryer was used on the cathode side in order to prevent formation of $H_3PO_4$ loss in the membrane structure by liquid water. After dryer, the air flow rate was controlled by the MFC of the test station for the flow rate set by user. The stack was cooled by thermo oil when it was needed, to the stack temperature set by user.

During the experiments, the three-way valves of test station were used to choose feeding gas. Before and after feeding reactant gasses to the HT-PEMFC stack throughout by test station, the stack was fed by $N_2$ gas driven by this three-way valve. The other inlets of this valve were pure $H_2$ and reformate gas mixture respectively.

### 3.4. Single PEMFC Test Procedure

Before begun performing test of the HT-PEMFC, it was necessary to check presence of short-circuit between the components of stack and then secondly perform gas leak test that may occur in the stack, connectors, fittings, or gas lines. The short circuit test was performed by using of multimeter. Once there was no short circuit, $N_2$ gas was fed at a flow rate of 1 slpm while keeping outlets of cathode and anode side of stack closed. If both the flow rate of $N_2$ and the pressure change on the pressurized line were zero, that meant there were not any gas leak.

Before starting the single HT-PEMFC performance tests, the gas lines were heated to 120°C and then, the single HT-PEMFC heated to the cell operating temperature. Once the temperature of the cell and gas lines has reached the desired values, the operation flow rates of the anode and cathode test gases $H_2$ and the dry air to the system were adjusted. The electronic load in the test system was switched on and maintained at a constant voltage of 0.7 V for 12 hours to condition the MEA structure. After conditioning, the single HT-PEMFC performance results were

measured for different voltage values. Then single cell was tested with reformate gas mixture and dry air to measure the performance of the cell.

In the cell closure method, the single HT-PEMFC voltage was set to a current density value of 0.1 A/cm$^2$ and the cell was cooled to 120°C. When the cell temperature reached 120°C, the current draw was terminated, and nitrogen gas was passed through the system and cooled to room temperature.

### 3.5. HT-PEMFC Preparation

The 300 W HT-PEMFC design was performed based on the single HT-PEMFC results. The operation cell voltage chosen as 0.6 V, because produced current decreases with increased cell voltage so the power requirement cannot be satisfied with high cell voltage. Also, when operation voltage less than the 0.5 V per cell can caused excess water generation according to concentration polarization dominated region of polarization curve. This excess water can block the operation of HT-PEMFC.

Gas flow rates, operating temperature, current, voltage and similar parameters of HT-PEMFC stack were determined. Although the fuel cell stack can be produced 300 W with the 10 cells when pure $H_2$ was supplied theoretically, it was decided to produce a 12 cell stack to compare with the reformed gas at the same condition. The pure $H_2$ was fed the stack with 5.95 slpm to feed 12 cells. The design of the HT-PEMFC within the scope of the thesis was evaluated for two different situations, assuming both the use of pure $H_2$ and the use of the reformate gas mixture. The flow rate calculation equations are given in APPENDIX B. The stack design results are given in Table 3.2.

Table 3.2. HT-PEMFC stack design parameters

| **Design Parameter** | **$H_2$** | **$H_2/CO_2/CO$** |
|---|---|---|
| Net Power | 300 W | 300 W |
| Design voltage | 0.6 V | 0.6 V |
| Current Density | 0.33 A/cm$^2$ | 0.28 A/cm$^2$ |
| Operation Temperature | 160°C | 160°C |
| Active area | 150 cm$^2$ | 150 cm$^2$ |
| Cell number | 10 | 12 |
| $P_{anode}$=$P_{cathode}$ | 1.2 atm | 1.2 atm |
| $T_{anode,inlet}$= $T_{cathode,inlet}$ | 120°C | 120°C |
| $T_{operation}$ | 160°C | 160°C |
| $H_2$: Air stoichiometry | 1.2:2.5 | 1.2:2.5 |
| Anode $H_2$ ratio | 100% | 75% |
| Anode $CO_2$ ratio | 0% | 22% |
| Anode CO ratio | 0% | 3% |
| $H_2$ flow rate | 5 slpm | - |
| Reformate gas flow rate | - | 6.74 slpm |
| Dry air flow rate | 29.63 slpm | 25 slpm |

After the design, 12 membranes of HT-PEMFC were prepared same as single HT-PEMFC. The catalyst was loaded on GDLs for an active area of 150 cm$^2$, such as on single cells to achieved high fuel cell performance. Then the MEAs of HT-PEMFC stack were produced at 150°C and 172 N/cm$^2$ for 10 minutes by hot press (Figure 3.5).

Figure 3.5.HT-PEMFC MEA (acid-leaching PBI membrane and GDE)

After preparation of MEAs, the flow channels of bipolar plates were designed in the Solidworks® CAD software program. Figure 3.6 shows the CAD drawing of the bipolar plates designed.

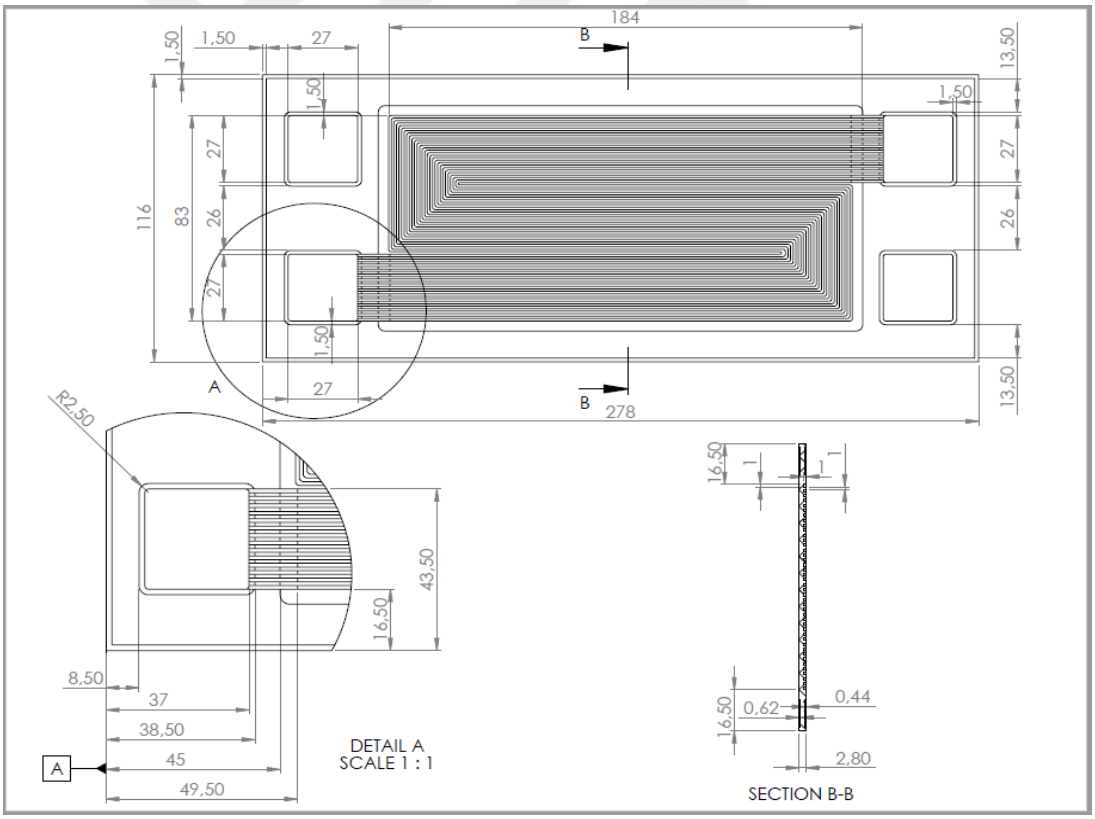


Figure 3.6. HT-PEMFC bipolar plate dimensions

After the drawing, the pressure drop in the flow channels of the bipolar plate was calculated using the Solidworks® Flow Simulation program. Assuming that, the reactant gases were distributed evenly to the cell with the help of manifolds, the flow rates to be fed to a single cell were measured and 3 different flow rates were compared. Then composite bipolar plates with the multiple parallel serpentine flow channel manufactured from composite graphite for HT-PEMFC stack as shown in Figure 3.7.

Figure 3.7.Composite graphite bipolar plate

Also, For the stack preparation the end plates and Viton® gaskets were produced as shown in Figure 3.8.

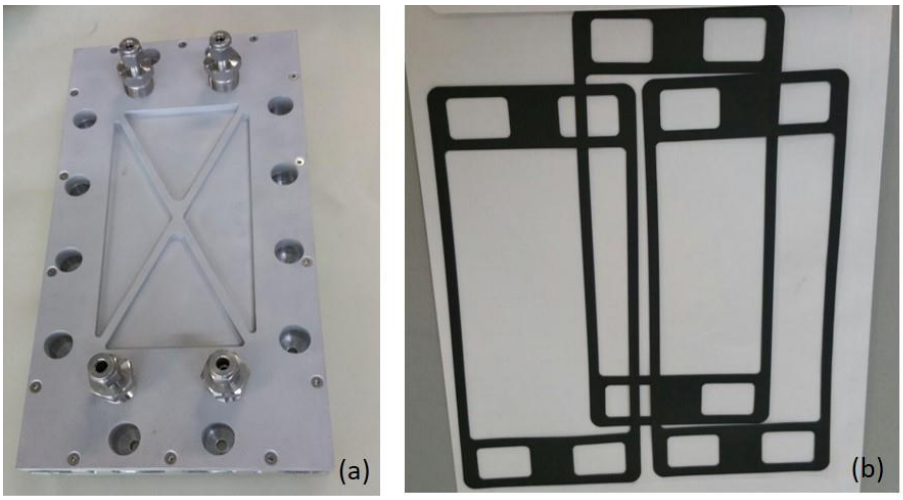


Figure 3.8.(a) Eloxal coated aluminum end plate (b) Viton® gasket

The three cooling plates which has five-port cooling channel were produced to control the stack temperature. The cooling plates which were arranged the stack as shown in the Figure 3.9 during the experiment. The thermo oil which was used as coolant liquid was passed inside the cooling plates. The thermo oil was fed to the system using the circulator. The HT-PEMFC stack temperature was efficiently controlled by the thermo-oil based cooling & heating system based upon on-off control system. For cooling the HT-PEMFC, the thermo oil has the average Cp value at 130ºC is 2.4 kJ/kgºC, the density is 840 kg/$m^3$, the viscosity is 0.00262 Pa (Ns)/$m^2$.

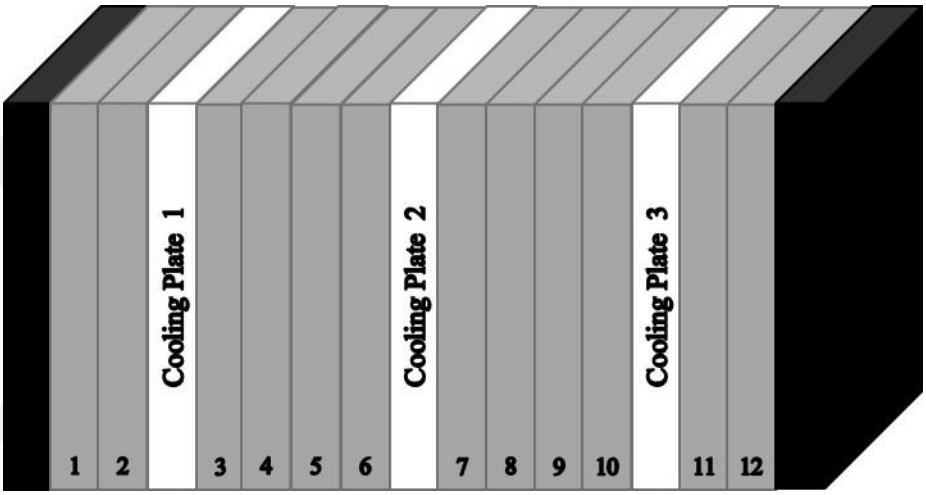


Figure 3.9.HT-PEMFC Cooling plates layout

The cooling liquid cooled the plates through an inverter (variable speed) pump. Depending on the operating power and temperature of the HT-PEMFC stack, the coolant flow rate can be adjusted. In the case of overheating or when the temperature falls below the operating temperature, the pump can switch on and off automatically.

HT-PEMFC stack combined with high-temperature work-resistant Viton® gaskets, cooling plates and gold-plated current collectors as shown in the Figure 3.10. Stainless steel fittings were used for the gas feeding and outlet connections. The stack has 1.7 Nm bolt load. The cooling liquid to be used during this cooling process was passed through the plates of the fuel cell with the help of an inverter circulating

pump. When the temperature in the system was above the desired limit, the fan was activated and provided additional cooling.

Figure 3.10. HT-PEMFC stack

### 3.6. HT-PEMFC Stack Test Procedure

HT-PEMFC stack and all gas lines were insulated with 1 cm glass wool to prevent undesired heat losses in the system. HT-PEMFC single cell tests were carried out by feeding pure $H_2$ to the anode side, then the same test was conducted by feeding reformate gas mixture to anode side instead of pure $H_2$. For both cases, the cathode side was fed by dry air at 160$^o$C. The HT-PEMFC stack working temperature was chosen 160$^o$C as an optimal value according to Devrim et. al. [54]. The dry reactants ($H_2$ or reformate gas ($H_2$/$CO_2$/CO;75/22/3)) was fed to the anode side ($\lambda_{anode}$: 1.2) and dry air was fed to the cathode side ($\lambda_{cathode}$: 2.5). Reactant gases were kept dry throughout the experiment. All performance tests were conducted under atmospheric pressure. Prior to testing, dry $N_2$ was used to verify if there was no reactive gas leakage.

At the beginning of the performance tests the HT-PEMFC stack was heated up to 120$^{o}$C in $N_2$ atmosphere. Stack heating was controlled with stack coolant under $N_2$ purge to prevent carbon corrosion caused by start-stop cycles. When the outlet temperature of the coolant increases until 120°C, reactant gases were fed to the stack. Before reactant gases could be supplied and starting the performance test, the temperatures of the stack and reactants were heated with the gas lines adjusted to 120$^{o}$C to minimize the acid leach problem caused by water in the liquid phase which may occur in the cathode side [46], [70].

When the stack temperature was increased to stack operation temperature, the performance tests were conducted. After the system was started, the electronic load was operated, and the system draws current. By maintaining a constant voltage for at least 12 hours, activation of the MEA structure was ensured. The VI curve was started to be taken for the test where the system has reached current changes below +/- 5 mA at constant voltage. During the test, the polarization curve and the power density curve were subtracted every six hours, the current change in the constant voltage, the change in the OCV was observed. When the test period was completed, $H_2$ and air gases entering the cell were closed first. Then the shutdown procedure was applied according to the international test protocols.

# CHAPTER 4

# 4. RESULTS

## 4.1. Single Cell Performance Results

A PBI membrane with a molecular weight of 82000 was synthesized and PVDF was used as a binder in the electrode. The acid doping level of the PBI membranes were 11 and the proton conductivities at 160ºC were 0.1030 S/cm.

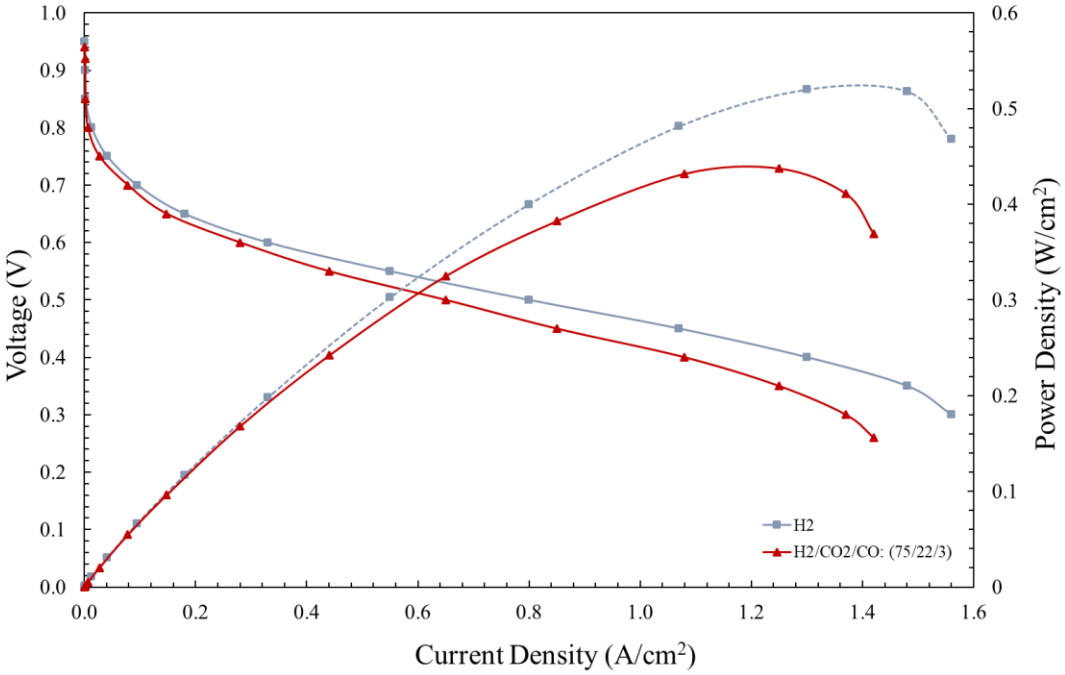


Figure 4.1.Single cell performance test results

The performance results of single cell were given in Figure 4.1. The current density values at 0.6 V were obtained as 0.33 A/cm$^2$ with pure $H_2$ supply and were observed as 0.28 A/cm$^2$ with reformate gas mixture supply at 160ºC.

This temperature was chosen because the experiments of Devrim et. al. shows that when the cell temperature increased, the cell performance also increased but at higher temperatures, it may cause other fatal problems such as deformation of other cell components like fittings [71]. The OCV value was observed as 0.98 V with pure $H_2$ and 0.94 with reformate gas mixture supply. This small change in OCV was based on the reformate gas mixture tests were performed with the same membranes after pure $H_2$ tests. This value was quite good values for PBI membrane because it showed the transmission of $H_2$ in the membrane was efficiently [20].

### 4.2. HT-PEMFC Bipolar Plate Flow Analysis Results

After the design of the stack, the pressure drop on the bipolar plate flow channel was analyzed using Solidworks® Flow Simulation program. In the HT-PEMFC stack, gas feeds were provided in parallel geometry of serpentine gas flow channels. This method assumed the equal gas distribution in overall bipolar plates. In Figure 4.2, Figure 4.3 and Figure 4.4, pressure distribution were provided for the supply of pure $H_2$ gas in bipolar plates at 0.5, 0.4 and 0.3 slpm, respectively.

The inlet pressures were measured as 121639 Pa, 121618 Pa, 121610 Pa and the pressure loss between the inlet and outlet manifold was calculated as 83.5 Pa, 66.76 Pa and 50.05 Pa, at 0.5, 0.4 and 0.3 slpm, respectively. No reverse flow was observed in the channels. All bipolar plates have same outlet pressure, so it was possible to evaluate how a flow rate effects pressure distribution. In the fastest gas flow, more pressure drop was observed. According to results 14 ea. parallel flow channel has unique (homogenous) gas distributions. Although more pressure drops at 0.5 slpm, more power can be generated with this flow rate. The forces that can be produced with flow rates were approximately 29.7 W, 24.7 W, and 18.15 W at 0.5, 0.4 and 0.3 slpm, respectively.

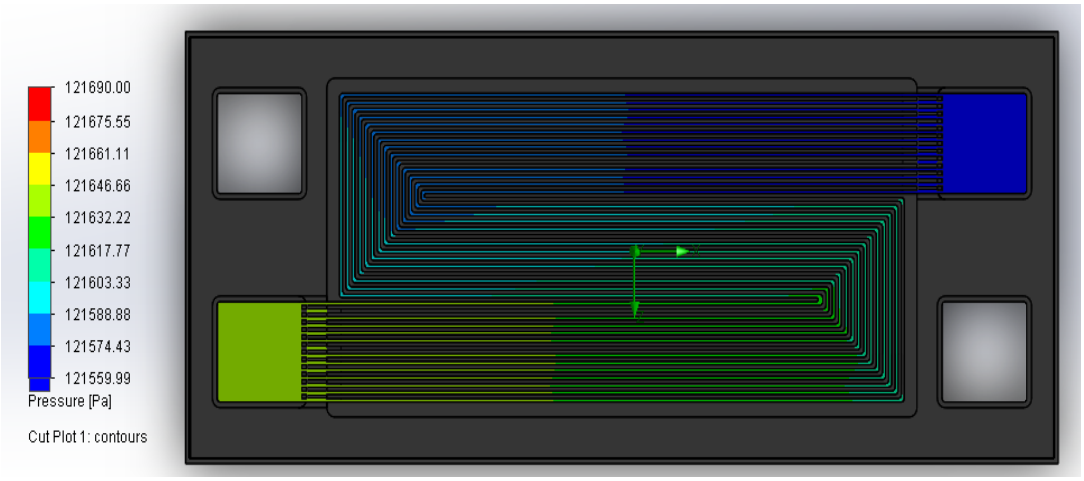


Figure 4.2. $H_2$ gas pressure difference in flow simulation with 0.5 slpm

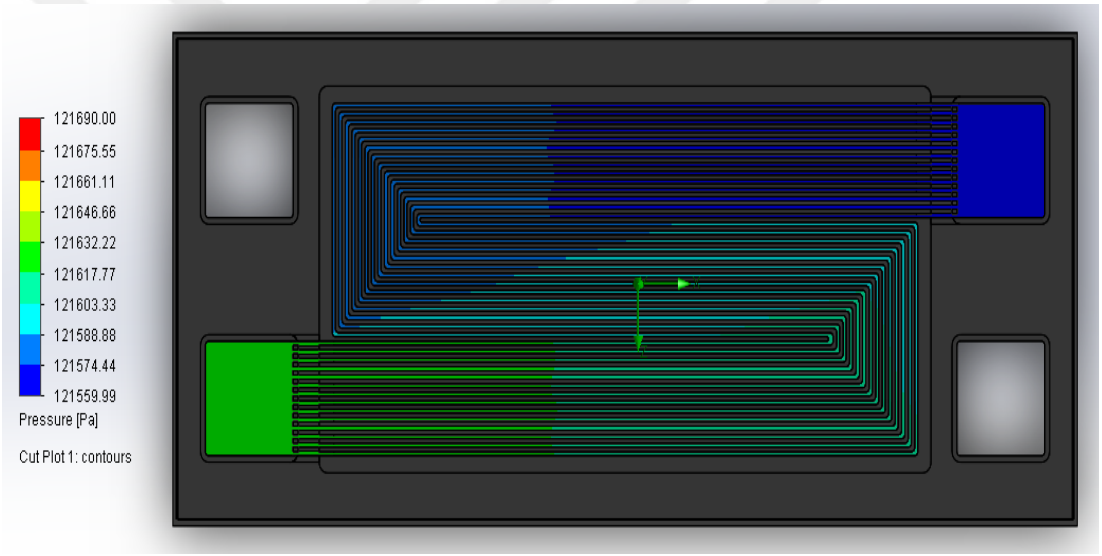


Figure 4.3. $H_2$ gas pressure difference in flow simulation with 0.4 slpm

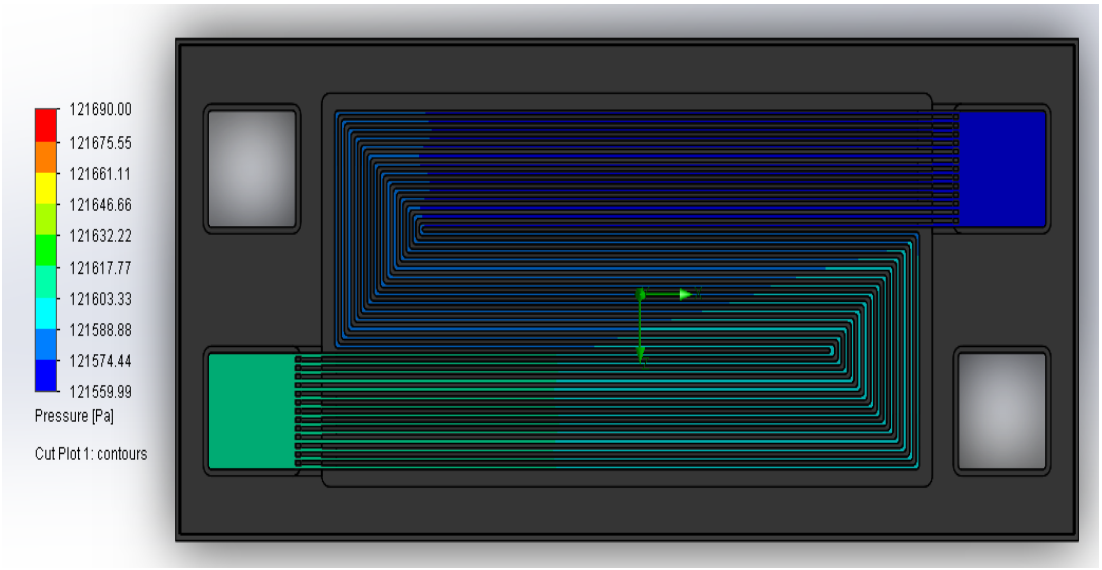


Figure 4.4.$H_2$ gas pressure difference in flow simulation with 0.3 slpm

Also, in the context of the thesis, gas flow analyzes were performed by using Solidworks® Flow Simulation program for bipolar plate channels in the case of comparative reforming gas supply. In order to produce net 300 W power, the amount of $H_2$ entering with the reformate gas mixture must be equal to that of pure $H_2$. For this reason, reformate gas mixture was supplied further into the system. Figure 4.5, Figure 4.6 and Figure 4.7 illustrate the reformate gas ($H_2$/$CO_2$/CO; 75/22/3) pressure distribution by the same geometry in bipolar plates for gas supply at 0.56, 0.46 and 0.36 slpm, respectively.

The inlet pressures were measured as 121689 Pa, 121674 Pa, 121621 Pa and the pressure loss between the inlet and outlet manifold were calculated as 129.83 Pa, 107.34 Pa and 62.17 Pa at 0.56, 0.46 and 0.36 slpm, respectively. No reverse flow was observed in the channels. In 14 ea. parallel gas channels, the speed distribution was uniformly acceptable. Although more pressure drops at 0.56 slpm, more power can be generated with this flow rate. The forces that can be produced with flow rates were approximately 25.2 W, 20.87 W and 16.47 W at 0.56, 0.46 and 0.36 slpm, respectively. Pressure differences in both reactant gases were very small considering the inlet and outlet pressures of the stack and therefore it can be ignored.

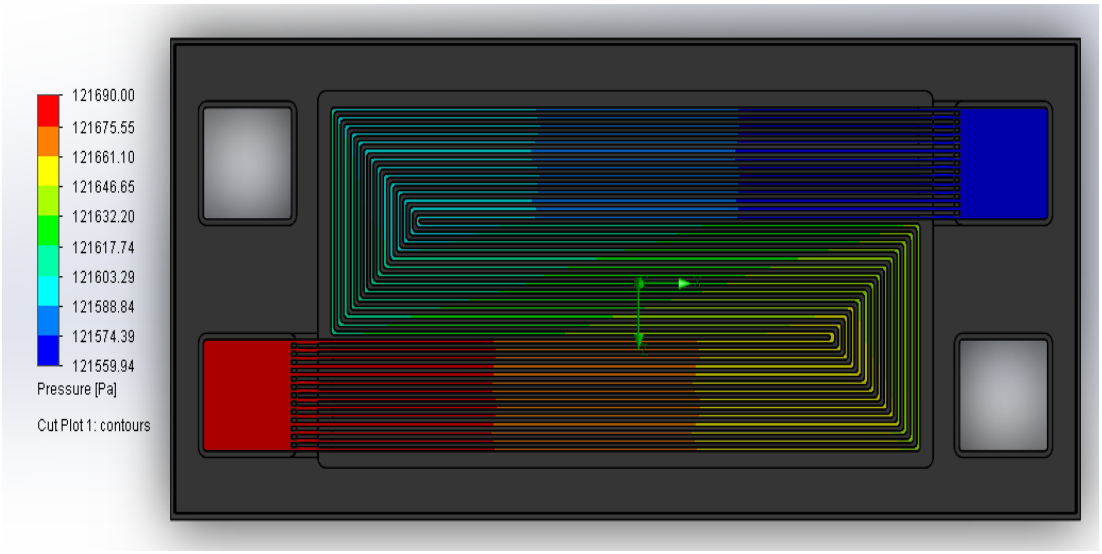


Figure 4.5.Reformate gas mixture pressure difference in flow simulation with 0.56 slpm

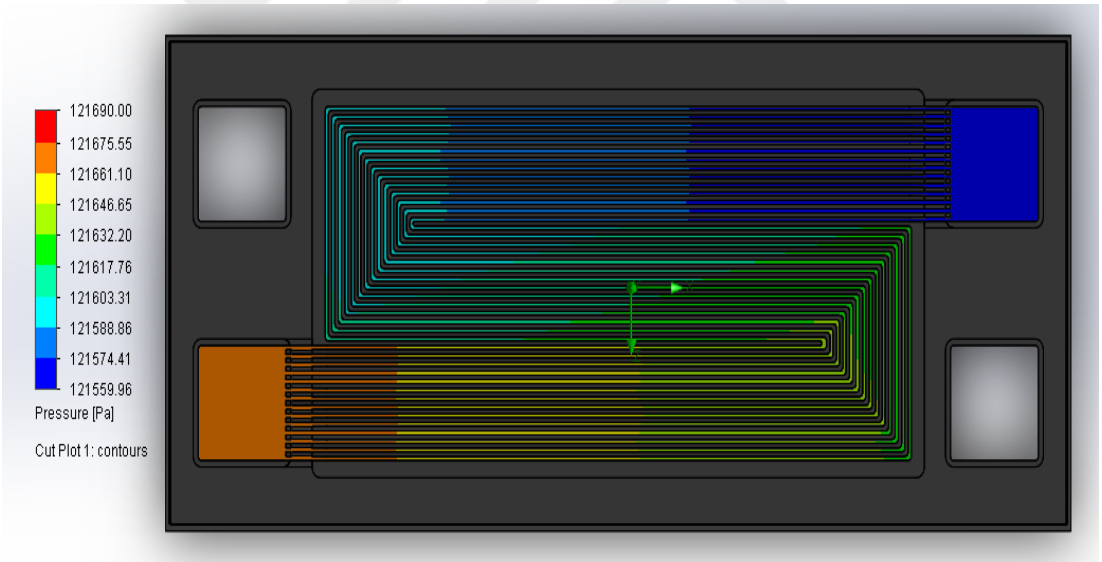


Figure 4.6. Reformate gas mixture pressure difference in flow simulation with 0.46 slpm

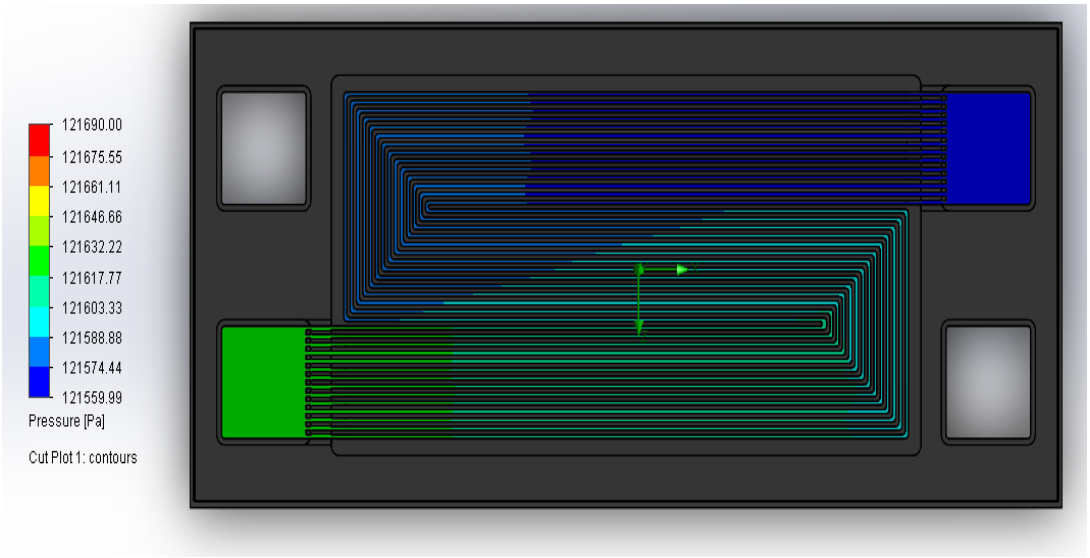


Figure 4.7. Reformate gas mixture pressure difference in flow simulation with 0.36 slpm

### 4.3. HT-PEMFC Stack Performance Test Results

The performance of stack was tested with both $H_2$ and reformate gas mixture in order to obtain effect of reformate gas on stack performance. In experiments with pure $H_2$ gas, the OCV value approximately ~ 0.93-0.95 V was obtained from each cell of HT-PEMFC. On the other hand, OCV values changed between ~ 0.925-0.95 V for the reformate gas mixture feeding by keeping all test parameters similar with the test of pure $H_2$ feeding. These results showed that the type of gas fed to the stack did not cause major changes in the OCV values obtained from the cells. The OCV change between the pure $H_2$ gas and reformate gas mixture was due to the feeding of the reformate gas mixture after feeding the $H_2$ as in single cell experiments.

Figure 4.8 compares the performance curves of the reformate gas mixture that includes $H_2/CO_2/CO$ with ratio 75/22/3 and the pure $H_2$ feeding at 160$^oC$ operating temperature of stack. When pure $H_2$ was fed as reactant gas to anode side, the stack produced 320 W power at 7.2 V stack voltage (0.6 V per cell) and the current was determined as 44.44 A. The cause of decreasing of current density was can be the stack resistance and reactant supply. The maximum power was obtained 468 W at 5.2 V (~0.43 V per cell). The HT-PEMFC stack power was determined as 281 W at

7.2 V stack voltage (0.6 V per cell) and the current was determined as 39 A. The maximum power obtained from the system was 423 W at 4.8 V (~0.4 V per cell). The current increases as the voltage decreases according to the polarization curve so the maximum power can be produced at lower cell voltage. The current increases as the voltage decreases according to the polarization curve so the maximum power can be produced at lower cell voltage.

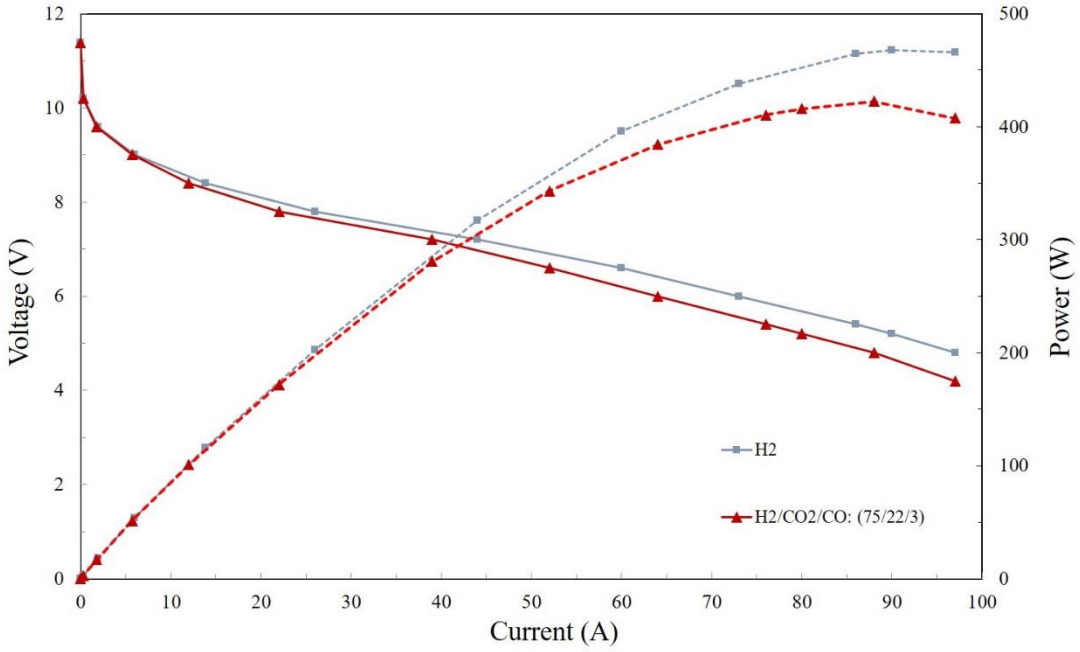


Figure 4.8. HT-PEMFC stack performance curves with $H_2$ and reformate gas mixture

It was evaluated that 12 % performance loss was observed when reformate gas mixture was fed comparing with the stack performance with pure $H_2$ feeding. This loss of performance may be occasioned by the reverse water-gas exchange reaction (RWGS) resulting in the conversion of $CO_2$ into CO, caused by the high operating temperature. Since PBI-based HT PEMFC operates without humidification, CO-electro-oxidation is neglected. The moisture-free supply of the anode gas stream exchanges the balance of CO formation with the reverse water-gas exchange reaction ($H_2 + CO_2 \rightarrow H_2O + CO$) [54]. The water formed due to this reaction may block the pores of the catalyst used in electrodes and cause loss of performance [72].

Studies conducted within the scope of the thesis yielded consistent results with the literature, and the main reason for the power difference between pure $H_2$ supply and reformed gas supply was the current densities produced at the same cell voltage.

During the tests, thermo oil was passed between the fluid plates at a flow rate of about 0.016 kg/s. The temperature of the cells was measured by temperature meters placed inside the bipolar plates. ± 5°C difference between cells at 7.2 V operating voltage. The most heated cells were the 5th and 8th cells which were not contact with the cooling plates, so that it was difficult to remove the reaction heat from these cells.

### 4.4. HT-PEMFC Stack Efficiency Results

The electrical efficiency of the HT-PEMFC stack is calculated by dividing the output power ($P_{out}$) of the stack by the input power which is supplied by the $H_2$ energy. $H_2$ energy equals the flow rate of inlet $H_2$ gas ($\dot{n}_{H_2}$) to be multiplied by low heating value ($\Delta h$=241.83 kJ/mol) [73];

$$\eta_{el} = \frac{P_{out}}{\dot{n}_{H_2} \times \Delta h} \tag{18}$$

The heat efficiency of stack is calculated by dividing the coolant power ($P_{coolant}$) of the stack by the chemical power of the $H_2$ ($P_{H_2}$). Coolant power equal to the multiplication of mass flow rates of PEMFC coolants ($\dot{m}_{cl}$), the specific temperatures of the coolant ($c_{p,cl}$) and the temperature change of the coolant ($\Delta T_{cl}$).

$$\eta_{heat} = \frac{P_{coolant}}{P_{H_2}} = \frac{\dot{m}_{cl} \times c_{p,cl} \times \Delta T_{cl}}{P_{H_2}} \tag{19}$$

Total stack efficiency is equal to sum of the electric efficiency and the thermal efficiency. The equation is given in below:

$$\eta_{total} = \eta_{el} + \eta_{heat} \tag{20}$$

The calculated electrical, heat and total efficiencies of stack for pure $H_2$ and reformat gas is given in Table 4.1. HT-PEMFC stack electrical, thermal and total efficiency values

Table 4.1. HT-PEMFC stack electrical, thermal and total efficiency values of the stack

| Membrane | Reactant gas* | $\eta_{el}$ (%) | $\eta_{heat}$ (%) | $\eta_{total}$ (%) |
|---|---|---|---|---|
| PBI | $H_2$: Dry air | 36 | 43 | 79 |
| PBI | ($H_2$:$CO_2$:CO): Dry air | 34 | 42 | 76 |

*6 slpm and 7 slpm anode flow rate were used for pure $H_2$ and reformate gas, respectively.

The stack electrical efficiency was calculated as 36 % for pure $H_2$ gas feeding. When the reformate gas mixture was fed to stack, the efficiency decreased to 34 %. For HT-PEMFC the total system efficiency could be increased if electrical efficiency and heat efficiency could be used at the same time by the μCHP application. The thermal efficiencies were calculated 43 % and 42 % for pure $H_2$ and reformate gas mixture respectively. With the use of reformate gas mixture, electrical efficiency of the stack decreases by 2 % and heat efficiency of the stack decreases by 1 %. The usage of reformate gas mixture as anode reactant has more effect on electrical efficiency than heat efficiency when compared with usage of pure $H_2$ as anode reactant.

# CHAPTER 5

## CONCLUSIONS

In the scope of the thesis, firstly $H_3PO_4$ doped PBI based proton exchange membranes were successfully synthesized for the HT-PEMFC. Then, single cell HT-PEMFC tests were performed with feeding of $H_2$ and $H_2/CO_2/CO$ as fuel at 160$^oC$. Following single cell testing, the stack was manufactured in order to test with a reformate gas mixture and the test system with a cooling system was upgraded. Depending on the result of single cell, HT-PEMFC stack were designed to produce 300W net power.

The design parameters were calculated and defined well and afterwards the solid CAD model were obtained by Solidworks®. CAD model was analyzed and simulated for stack working conditions and the limitations were defined and some iterations performed on the design of stack. During computer aided analysis, pressure drop of reactant gas analysis were performed for bipolar plates gas distribution channels with using suitable modules of Solidworks® Flow Simulation program at three different flow rates for $H_2$ and reformate gas mixture. In these analyzes, it was chosen that the flow rates were 0.5 and 0.56 for $H_2$ and reformate gas mixture, respectively. These chosen flow rates were preferred even these had the highest pressure drops because these flow rates provided the theoretical highest power generation rates on the analysis. Before the performance tests of HT-PEMFC, it was determined that the materials used in the HT-PEMFC stack and in the design of the stack did not cause any gas leakage or short circuit problem. Also, the stack insulation made by using 1 cm glass wool reduced the temperature difference between the cells and a more efficient cooling.

After the analysis, 12 cell HT-PEMFC stack with 150 $cm^2$ active area/cell was manufactured. When $H_2$ and dry air gases feed to the PBI membrane based MEA, 320 W of power was obtained from the system at 7.2 V stack voltage and the current was determined as ~ 44.44 A. In the case of reformate gas mixture 281 W power was obtained from the system at 7.2 V stack voltage and the current was determined as ~ 39 A.

The maximum power was obtained higher than the designed power which was equal 468 W at 5.2 V (~0.43 V per cell). When the reformate gas mixture containing $H_2/CO_2/CO$ (75/22/3) was used, the maximum power value obtained from the system was 423 W at 4.8 V (~0.4 V per cell). The performance loss at 7.2 V was observed as 12 % in the case of reformate gas mixture. The loss increased to approximately 9.6 % when the maximum powers were considered.

As a result of the calculations, 36 % electrical efficiency was obtained when pure $H_2$ was fed with 1.2 stoichiometry. When the reformate gas mixture was fed in the systems, the electrical efficiency was determined as 34 %. The stack total efficiencies can be increased to 79 % and 76 % with pure $H_2$ and reformate gas $H_2/CO_2/CO$ (75/22/3), respectively by μCHP application.

In order to develop the project, the following subjects can be emphasized in the following studies:

- Composite membrane can be prepared and its effects on proton conductivity can be examined.
- The effects of membranes prepared with different conductivity and qualities can be realized by examining the effects of membranes prepared by the project with acids other than phosphoric acid (sulfuric acid, phosphonic acid etc.).
- In order to increase performance in high temperature applications, optimization in both MEA preparation conditions and fuel cell operation conditions would be good for increasing performance.

- The HT-PEMFC performances can be analyzed by reformer integration the system and μCHP application.

## REFERENCES


[1] A. Midilli, M. Ay, I. Dincer, and M. A. Rosen, 'On hydrogen and hydrogen energy strategies I : Current status and needs', Renew. Sustain. Energy Rev., vol. 9, no. 3, pp. 255–271, 2005.

[2] M. Y. F. A. Mustafa, 'Design and manufacturing of a ( PEMFC ) proton exchange membrane fuel cell', Coventry University, 2009.

[3] A. Kirubakaran, S. Jain, and R. K. Nema, 'A review on fuel cell technologies and power electronic interface', Renewable and Sustainable Energy Reviews, vol. 13, no. 9. pp. 2430–2440, 2009.

[4] P. Grimes, 'Historical pathways for fuel cells. The new electric century', Proc. Annu. Batter. Conf. Appl. Adv., pp. 41–45, 2000.

[5] F. Barbir, PEM fuel cells : Theory and practice. Elsevier, 2013.

[6] S. Mekhilef, R. Saidur, and A. Safari, 'Comparative study of different fuel cell technologies', Renewable and Sustainable Energy Reviews, vol. 16, no. 1. Elsevier Ltd, pp. 981–989, 2012.

[7] M. W. Ellis, M. R. Von Spakovsky, and D. J. Nelson, 'Fuel cell systems: Efficient, flexible energy conversion for the 21st century', Proc. IEEE, vol. 89, no. 12, pp. 1808–1817, 2001.

[8] S. Pehlivan-Davis, 'Polymer Electrolyte Membrane (PEM) fuel cell seals durability', Loughborough University, 2015.

[9] E. Stambouli, A. B. and Traversa, 'Solid oxide fuel cells (SOFCs): a review of an environmentally clean and efficient source of energy.', Renew. Sustain. Energy Rev., vol. 6, no. 5, pp. 433–455, 2002.

[10] S. Yerramalla, A. Davari, A. Feliachi, and T. Biswas, 'Modeling and simulation of the dynamic behavior of a polymer electrolyte membrane fuel cell', J. Power Sources, vol. 124, no. 1, pp. 104–113, 2003.

[11] E. Mancusi, E. Fontana, A. A. Ulson De Souza, and S. M. A. Guelli Ulson De Souza, 'Numerical study of two-phase flow patterns in the gas channel of PEM fuel cells with tapered flow field design', Int. J. Hydrogen Energy, vol. 39, no. 5, pp. 2261–2273, 2014.

[12] 'Comparison of fuel cell technologies'. [Online]. Available: https://www.energy.gov/eere/fuelcells/comparison-fuel-cell-technologies. [Accessed: 04-Jan-2018].

[13] C. Spiegel, Designing and building fuel Cells. United States of America: The McGraw-Hill Companies, 2007.

[14] I. Pilatowsky, R. J. Romero, C. A. Isaza, S. A. Gamboa, P. J. Sebastian, and W. Rivera, 'Thermodynamics of fuel ells', in Cogeneration Fuel Cell-Sorption Air Conditioning Systems, 2011, pp. 25–36.

[15] J. H. Jung and S. Ahmed, 'Dynamic model of PEM fuel cell using real-time simulation techniques', J. Power Electron., vol. 10, no. 6, pp. 739–748, 2010.

[16] J. Zhang, Ed., PEM fuel cell electrocatalysts and catalyst layers. Springer, 2008.

[17] S. J. Peighambardoust, S. Rowshanzamir, and M. Amjadi, Review of the proton exchange membranes for fuel cell applications, vol. 35, no. 17. Elsevier Ltd, 2010.

[18] Y. Bahramzadeh and M. Shahinpoor, 'A review of ionic polymeric soft actuators and sensors', Soft Robot., vol. 1, no. 1, pp. 38–52, 2013.

[19] T. Sata, Ion exchange membranes preparation, characterization, modification and application. The Royal Society of Chemistry, 2004.

[20] Y. Özdemir, N. Özkan, and Y. Devrim, 'Fabrication and characterization of cross-linked polybenzimidazole based membranes for high temperature PEM fuel cells', Electrochim. Acta, vol. 245, pp. 1–13, 2017.

[21] J. Mader, L. Xiao, T. J. Schmidt, and B. C. Benicewicz, 'Polybenzimidazole/Acid complexes as high-temperature membranes', in Advances in Polymer Science, 2008, pp. 63–124.

[22] J. Mader, L. Xiao, T. J. Schmidt, B. Fuel, and V. Ave, Polybenzimidazole/Acid complexes as high-temperature membranes in fuel cells II, no. February. Berlin,Germany: Advances in Polymer Science, 2008.

[23] R. Zeis, 'Materials and characterization techniques for high-temperature polymer electrolyte membrane fuel cells', Beilstein J. Nanotechnol., vol. 6, no. 1, pp. 68–83, 2015.

[24] H. RONGHUAN, Q. LI, J. O. JENSEN, and N. J. BJERRU, 'Doping phosphoric acid in polybenzimidazole membranes for high temperature proton exchange membrane fuel cells', J. Polym. Sci. Part A Polym. Chem., vol. 45, pp. 2989–2997, 2007.

[25] S. S. Araya et al., 'A comprehensive review of PBI-based high temperature PEM fuel cells', Int. J. Hydrogen Energy, vol. 41, no. 46, pp. 21310–21344, 2016.

[26] S. Holdcroft, 'Fuel cell catalyst layers: A polymer science perspective', Chem. Mater., vol. 26, no. 1, pp. 381–393, 2014.

[27] Y. Devrim, S. Erkan, N. Baş, and I. Eroglu, ‘Improvement of PEMFC performance with Nafion/inorganic nanocomposite membrane electrode assembly prepared by ultrasonic coating technique’, Int. J. Hydrogen Energy, vol. 37, no. 21, pp. 16748–16758, 2012.

[28] B. G. Pollet, ‘The use of ultrasound for the fabrication of fuel cell materials’, Int. J. Hydrogen Energy, vol. 35, no. 21, pp. 11986–12004, 2010.

[29] A. Jayakumar, S. Singamneni, M. Ramos, A. M. Al-Jumaily, and S. S. Pethaiah, ‘Manufacturing the gas diffusion layer for PEM fuel cell using a novel 3D printing technique and critical assessment of the challenges encountered’, Materials (Basel)., vol. 10, no. 7, pp. 1–9, 2017.

[30] A. Hermann, T. Chaudhuri, and P. Spagnol, ‘Bipolar plates for PEM fuel cells: A review’, Int. J. Hydrogen Energy, vol. 30, no. 12, pp. 1297–1302, 2005.

[31] V. V. Nikam, R. G. Reddy, S. R. Collins, P. C. Williams, G. H. Schiroky, and G. W. Henrich, ‘Corrosion resistant low temperature carburized SS 316 as bipolar plate material for PEMFC application’, Electrochim. Acta, vol. 53, no. 6, pp. 2743–2750, 2008.

[32] R. Taherian, ‘A review of composite and metallic bipolar plates in proton exchange membrane fuel cell: Materials, fabrication, and material selection’, J. Power Sources, vol. 265, pp. 370–390, 2014.

[33] J. W. Patrick, ‘Handbook of fuel cells. Fundamentals technology and applications’, Fuel, vol. 83, no. 4–5, p. 623, 2003.

[34] Y. A. Dobrovol’skii et al., ‘Materials for bipolar plates for proton-conducting membrane fuel cells’, Russ. J. Gen. Chem., vol. 77, no. 4, pp. 752–765, 2007.

[35] S. H. Wang, J. Peng, W. B. Lui, and J. S. Zhang, ‘Performance of the gold-plated titanium bipolar plates for the light weight PEM fuel cells’, J. Power Sources, vol. 162, no. 1, pp. 486–491, 2006.

[36] T. M. Besmann, J. J. Henry, J. W. Klett, and E. Lara-Curzio, ‘Carbon/ Carbon composite bipolar plate for PEM fuel cells’, Carbon N. Y., no. 2, p. 114, 2001.

[37] X. Li and I. Sabir, ‘Review of bipolar plates in PEM fuel cells: Flow-field designs’, Int. J. Hydrogen Energy, vol. 30, no. 4, pp. 359–371, 2005.

[38] Y. Tang, W. Yuan, M. Pan, and Z. Wan, ‘Feasibility study of porous copper fiber sintered felt: A novel porous flow field in proton exchange membrane fuel cells’, Int. J. Hydrogen Energy, vol. 35, no. 18, pp. 9661–9677, 2010.

[39] N. Ul Hassan, M. Kilic, E. Okumus, B. Tunaboylu, and A. M. Soydan, ‘Experimental determination of optimal clamping torque for AB-PEM fuel cell’, J. Electrochem. Sci. Eng., vol. 6, no. 1, p. 9, 2016.

[40] S. Shimpalee, S. Greenway, and J. W. Van Zee, ‘The impact of channel path length on PEMFC flow-field design’, J. Power Sources, vol. 160, no. 1, pp. 398–406, 2006.

[41] J. Wang, J. Yan, J. Yuan, and B. Sundén, ‘On flow maldistribution in PEMFC stacks’, Int. J. Green Energy, vol. 8, no. 5, pp. 585–606, 2011.

[42] G. Zhang and S. G. Kandlikar, ‘A critical review of cooling techniques in proton exchange membrane fuel cell stacks’, Int. J. Hydrogen Energy, vol. 37, no. 3, pp. 2412–2429, 2012.

[43] S. M. H. Hashmi, ‘Cooling strategies for PEMFC stacks’, Helmut Schmidt University / University of the Federal Armed Forces Hamburg, 2010.

[44] R. K. Abdul Rasheed, Q. Liao, Z. Caizhi, and S. H. Chan, ‘A review on modelling of high temperature proton exchange membrane fuel cells (HT-PEMFCs)’, Int. J. Hydrogen Energy, vol. 42, no. 5, pp. 3142–3165, 2017.

[45] Y. Liu, W. Lehnert, H. Janßen, R. C. Samsun, and D. Stolten, ‘A review of high-temperature polymer electrolyte membrane fuel-cell (HT-PEMFC)-based auxiliary power units for diesel-powered road vehicles’, J. Power Sources, vol. 311, pp. 91–102, 2016.

[46] R. E. Rosli et al., ‘A review of high-temperature proton exchange membrane fuel cell (HT-PEMFC) system’, Int. J. Hydrogen Energy, vol. 42, no. 14, pp. 9293–9314, 2017.

[47] D. D. Boettner and M. J. Moran, ‘Proton exchange membrane (PEM) fuel cell-powered vehicle performance using direct-hydrogen fueling and on-board methanol reforming’, Energy, vol. 29, no. 12–15 SPEC. ISS., pp. 2317–2330, 2004.

[48] H. R. Ellamla, I. Staffell, P. Bujlo, B. G. Pollet, and S. Pasupathi, ‘Current status of fuel cell based combined heat and power systems for residential sector’, J. Power Sources, vol. 293, pp. 312–328, 2015.

[49] E. Jannelli, M. Minutillo, and A. Perna, ‘Analyzing microcogeneration systems based on LT-PEMFC and HT-PEMFC by energy balances’, Appl. Energy, vol. 108, pp. 82–91, 2013.

[50] Y. Garsany, B. D. Gould, O. A. Baturina, and K. E. Swider-Lyons, ‘Comparison of the sulfur poisoning of PBI and Nafion PEMFC cathodes’, Electrochem. Solid-State Lett., vol. 12, no. 9, pp. B138–B140, 2009.

[51] L. Barelli, G. Bidini, F. Gallorini, and A. Ottaviano, ‘An energetic-exergetic analysis of a residential CHP system based on PEM fuel cell’, Appl. Energy, vol. 88, no. 12, pp. 4334–4342, 2011.

[52] F. B. Weng, C. K. Cheng, C. Y. Lee, and C. P. Chang, ‘Analysis of thermal balance in high-temperature proton exchange membrane fuel cells with short

stacks via in situ monitoring with a flexible micro sensor', Int. J. Hydrogen Energy, vol. 39, no. 25, pp. 13681–13686, 2014.

[53] S. Authayanun and V. Hacker, 'Energy and exergy analyses of a stand-alone HT-PEMFC based trigeneration system for residential applications', Energy Convers. Manag., vol. 160, no. August 2017, pp. 230–242, 2018.

[54] Y. Devrim, A. Albostan, and H. Devrim, 'Experimental investigation of CO tolerance in high temperature PEM fuel cells', Int. J. Hydrogen Energy, vol. 43, no. 40, pp. 18672–18681, 2018.

[55] S. J. Andreasen and S. K. Kær, '400 W high temperature PEM fuel cell stack test', ECS Trans., vol. 5, no. 1, pp. 197–207, 2007.

[56] N. Zuliani and R. Taccani, 'Microcogeneration system based on HTPEM fuel cell fueled with natural gas: Performance analysis', Appl. Energy, vol. 97, pp. 802–808, 2012.

[57] E. Harikishan Reddy and S. Jayanti, 'Thermal management strategies for a 1 kWe stack of a high temperature proton exchange membrane fuel cell', Appl. Therm. Eng., vol. 48, pp. 465–475, 2012.

[58] C. H. Yang and W. L. Wang, 'A kW level high temperature proton exchange membrane fuel cell stack and its cooling technique', 2016 IEEE Int. Conf. Power Renew. Energy, ICPRE 2016, pp. 200–203, 2017.

[59] A. Jo et al., 'Modeling and analysis of a 5 kWe HT-PEMFC system for residential heat and power generation', Int. J. Hydrogen Energy, vol. 42, no. 3, pp. 1698–1714, 2017.

[60] J. Renau et al., 'Design and manufacture of a high-temperature PEMFC and its cooling system to power a lightweight UAV for a high altitude mission', Int. J. Hydrogen Energy, vol. 41, no. 43, pp. 19702–19712, 2016.

[61] G. Giacoppo et al., '1.5 kWe HT-PEFC stack with composite MEA for CHP application', Int. J. Hydrogen Energy, vol. 38, no. 26, pp. 11619–11627, 2013.

[62] Y. Nalbant, C. O. Colpan, and Y. Devrim, 'Development of a one-dimensional and semi-empirical model for a high temperature proton exchange membrane fuel cell', Int. J. Hydrogen Energy, vol. 43, no. 11, pp. 5939–5950, 2018.

[63] V. Mehta and J. S. Cooper, 'Review and analysis of PEM fuel cell design and manufacturing', J. Power Sources, vol. 114, no. 1, pp. 32–53, 2003.

[64] A. Ghosh and A. Verma, 'Carbon-polymer composite bipolar plate for HT-PEMFC', Fuel Cells, vol. 14, no. 2, pp. 259–265, 2014.

[65] P. Graphite, 'Pyrocell bipolar plates', 2014. [Online]. Available: http://poco.com/industriesapplications/industrial/fuelcell.aspx. [Accessed: 26-Jan-2019].

[66] M. Erni, W. D. Wan Ramli, and M. Edy Herianto, ‘Review on serpentine flow field design for PEM fuel cell system’, Key Eng. Mater., vol. 447–448, pp. 559–563, 2010.

[67] J. Kim, J. Park, Y. Kim, S. Ahn, H. Sun, and K. Kim, ‘Fuel cell end plates : A review’, vol. 9, no. 1, pp. 39–46, 2008.

[68] Y. Özdemir, N. Üregen, and Y. Devrim, ‘Polybenzimidazole based nanocomposite membranes with enhanced proton conductivity for high temperature PEM fuel cells’, Int. J. Hydrogen Energy, vol. 42, no. 4, pp. 2648–2657, 2017.

[69] Y. Devrim, H. Devrim, and I. Eroglu, ‘Polybenzimidazole/SiO2 hybrid membranes for high temperature proton exchange membrane fuel cells’, Int. J. Hydrogen Energy, vol. 41, no. 23, pp. 10044–10052, 2016.

[70] Q. Li, C. Pan, J. O. Jensen, P. Noyé, and N. J. Bjerrum, ‘Cross-linked polybenzimidazole membranes for fuel cells’, Chem. Mater., vol. 19, no. 3, pp. 350–352, 2007.

[71] Y. Devrim, A. Albostan, and H. Devrim, ‘Experimental investigation of CO tolerance in high temperature PEM fuel cells’, Int. J. Hydrogen Energy, vol. 3, pp. 0–9, 2018.

[72] M. Boaventura, I. Alves, P. Ribeirinha, and A. Mendes, ‘The influence of impurities in high temperature polymer electrolyte membrane fuel cells performance’, Int. J. Hydrogen Energy, vol. 41, no. 43, pp. 19771–19780, 2016.

[73] Y. Budak and Y. Devrim, ‘Investigation of micro-combined heat and power application of PEM fuel cell systems’, Energy Convers. Manag., vol. 160, no. January, pp. 486–494, 2018.

[74] N. Üregen, K. Pehlivanoğlu, Y. Özdemir, and Y. Devrim, ‘Development of polybenzimidazole/graphene oxide composite membranes for high temperature PEM fuel cells’, Int. J. Hydrogen Energy, vol. 42, no. 4, pp. 2636–2647, 2017.

# APPENDIX A

## A.1.PBI MEMBRANE ACID DOPING LEVEL AND ACID LOSS PERCENTAGE

Acid doping levels of the membrane is calculated according to the given equation:

$$\text{Acid Doping Level} = \frac{W_{H3PO4}}{W_{dry}} \times \frac{\text{MWofPBIRepeatUnit}}{\text{MWof}H_3PO_4} \quad (21)$$

Where $W_{H3PO4}$ is the weight of membrane after acid doped process, $W_{dry}$ is the weight of membrane before acid doped process.

After the acid leaching test, acid loss percentages of the membrane was calculated according to the given equation [74]:

$$\text{Acid Loss Percentage} = \frac{W_o - W_i}{W_a} \quad (22)$$

Where $W_0$ is the initial weight of acid doped membrane, Wa is the weight of $H_3PO_4$ present in the membrane and Wi is the weight of the $H_3PO_4$ doped membrane after leaching.

## APPENDIX B

### B.1.HT-PEMFC FLOW RATES

$H_2$ is feed to the stack from the anode side. $N_{H_2}$ is $H_2$ molar flow rate which is contingent upon the stoichiometric ratio of $H_2$ ($S_{H_2}$), $r_{co2}$ is $CO_2$ volume in reformat gas, $r_{co}$ is CO volume in reformat gas, $r_{H2}$ is $H_2$ volume in reformat gas, cell area A ($cm^2$), current density I ($A/cm^2$) and $N_{cell}$ is cell number. The $H_2$, $CO_2$ and CO molar flow rate at the anode gas inlet of the PEMFC calculated in below equation:

$$N_{H_2}=\frac{S_{H_2}}{r_{H2}}\times\frac{I\times A}{2\times F}\times N_{cell} \tag{23}$$

$$N_{CO_2}=\frac{S_{H_2}}{r_{o2}}\times r_{CO_2}\times\frac{I\times A}{2\times F}\times N_{cell} \tag{24}$$

$$N_{CO}=\frac{S_{H_2}}{r_{o2}}\times r_{CO}\times\frac{I\times A}{2\times F}\times N_{cell} \tag{25}$$

Air is feed to the stack from the cathode side. $N_{O_2}$ is $O_2$ molar flow rate and depends on the stoichiometric ratio $S_{O_2}$, $r_{O_2}$ is $O_2$ volume in air that is 21 %. The $O_2$ and air molar flow rate at the cathode inlet of the HT-PEMFC can be calculated as follows:

$$N_{O_2}=S_{O_2}\times\frac{I\times A}{4\times F}\times N_{cell} \tag{26}$$

$$N_{air}=\frac{S_{O_2}}{r_{O_2}}\times\frac{I\times A}{4\times F}\times N_{cell} \tag{27}$$

HT- PEMFC's energy balance equation is given in the following equation:

$$\sum \dot{E}_{mass,in}-\sum \dot{E}_{mass,out}+\dot{Q}-\dot{W}_{net}=0 \tag{28}$$

where $\Sigma\dot{E}_{mass,in}$ is total enthalpy of inlet gases, $\Sigma\dot{E}_{mass,out}$ is total enthalpy of outlet gases of HT-PEMFC. Q is heat dissipation from stacks to ambient. $W_{net}$ is net power production from stack.